Molecular Therapy
Methods & Clinical Development
Original Article

Subretinal AAV delivery of RNAi-therapeutics targeting *VEGFA* reduces choroidal neovascularization in a large animal model

Silja Hansen Haldrup,[1] Bjørn K. Fabian-Jessing,[1,2,3] Thomas Stax Jakobsen,[1,2,3] Anna Bøgh Lindholm,[1] Rikke L. Adsersen,[1] Lars Aagaard,[1] Toke Bek,[2] Anne Louise Askou,[1,2] and Thomas J. Corydon[1,2]

[1]Department of Biomedicine, Aarhus University, Høegh-Guldbergs Gade 10, 8000 Aarhus C, Denmark; [2]Department of Ophthalmology, Aarhus University Hospital, Palle Juul-Jensens Boulevard 167, 8200 Aarhus N, Denmark

Neovascular age-related macular degeneration (nAMD) is a frequent cause of vision loss among the elderly in the Western world. Current disease management with repeated injections of anti-VEGF agents accumulates the risk for adverse events and constitutes a burden for society and the individual patient. Sustained suppression of VEGF using gene therapy is an attractive alternative, which we explored using adeno-associated virus (AAV)-based delivery of novel RNA interference (RNAi) effectors in a porcine model of choroidal neovascularization (CNV). The potency of *VEGFA*-targeting, Ago2-dependent short hairpin RNAs placed in pri-microRNA scaffolds (miR-agshRNA) was established *in vitro* and *in vivo* in mice. Subsequently, AAV serotype 8 (AAV2.8) vectors encoding *VEGFA*-targeting or irrelevant miR-agshRNAs under the control of a tissue-specific promotor were delivered to the porcine retina via subretinal injection before CNV induction by laser. Notably, *VEGFA*-targeting miR-agshRNAs resulted in a significant and sizable reduction of CNV compared with the non-targeting control. We also demonstrated that single-stranded and self-complementary AAV2.8 vectors efficiently transduce porcine retinal pigment epithelium cells but differ in their transduction characteristics and retinal safety. Collectively, our data demonstrated a robust anti-angiogenic effect of *VEGFA*-targeting miR-aghsRNAs in a large translational animal model, thereby suggesting AAV-based delivery of anti-VEGFA RNAi therapeutics as a valuable tool for the management of nAMD.

INTRODUCTION

Age-related macular degeneration (AMD) is a frequent cause of vision loss among elderly people in the Western world.[1,2] In the USA and Europe, approximately 20 million and 65 million individuals are currently affected by AMD, respectively, and of these about 1.5 million and 10 million suffer from late-stage disease.[3,4] These numbers will increase with the aging of the populations.[3] In the neovascular form of the disease, new blood vessels of choroidal origin penetrate Bruch's membrane and form neovascular membranes in the subretinal pigment epithelium (RPE) or subretinal space. These choroidal neovascularizations (CNVs) cause structural retinal damage ultimately leading to irreversible vision loss.[5] Vascular endothelial growth factor (VEGF) is a key factor in disease pathogenesis and current treatment with intravitreal administration of anti-VEGF agents has dramatically improved the prognosis.[6–8] However, the requirement of frequent injections accumulates accompanying risks and provides a significant burden for both society and the individual patient. Hence, novel durable treatment strategies are desirable. A promising strategy for permanent VEGF suppression is gene therapy. Indeed, this strategy is currently being investigated in several clinical trials. In the majority of these, subretinal or intravitreal delivery of adeno-associated virus (AAV) vectors encoding anti-VEGF agents are pursued. Examples include delivery of the VEGF neutralizing soluble FLT-1 receptor,[9,10] aflibercept,[11] or a monoclonal antibody fragment similar to ranibizumab.[12,13]

Another strategy to achieve sustained VEGF suppression is RNA interference (RNAi) technology. RNAi is a mechanism of posttranscriptional gene regulation, mediated by small double-stranded RNA effector molecules interacting with specific mRNA transcripts through complementary base pairing.[14,15] For therapeutic purposes, promotor-driven short hairpin RNAs (shRNAs) enable stable expression of RNAi therapeutics in mammalian cells. This allows them to be harnessed for specific and sustained gene suppression.[16–18] Unfortunately, this strategy suffers from the risk of off-target effects, in which unintended sequence complementarity of the guide strand and/or the co-delivered passenger strand to non-targeted genes may lead to unintentional gene silencing.[19] Furthermore, oversaturation of the endogenous microRNA (miRNA) pathway by competing shRNAs may lead to

Received 11 October 2023; accepted 21 March 2024;
https://doi.org/10.1016/j.omtm.2024.101242.

[3]These authors contributed equally

Correspondence: Thomas Corydon, Department of Biomedicine, Aarhus University, Høegh-Guldbergs Gade 10, 8000 Aarhus C, Denmark.
E-mail: corydon@biomed.au.dk

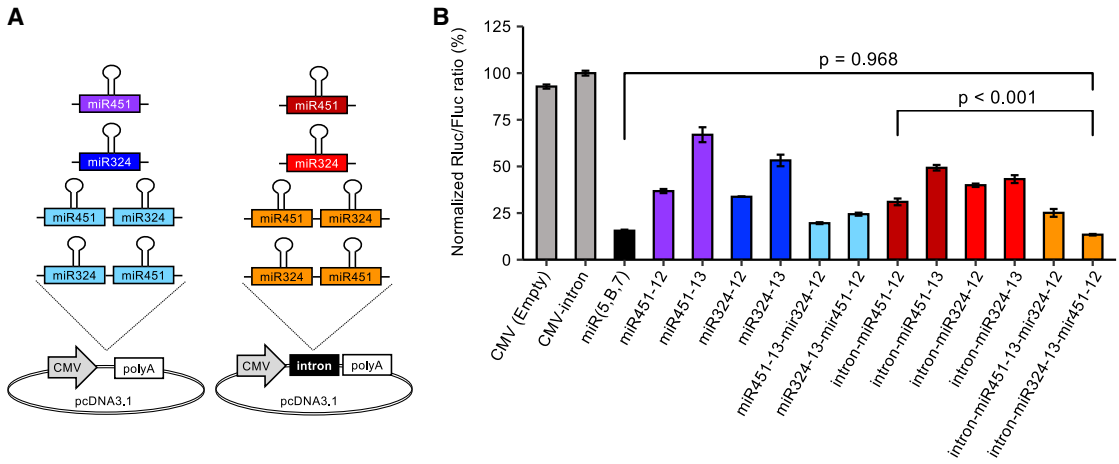

Figure 1. Design and knockdown efficacy of *Vegfa* targeting miR-agshRNA constructs

(A) Schematic diagram of the miR-agshRNA units tested with or without intron embedment in pcDNA3.1-based plasmids. (B) Bar plot (mean ± SD) showing *Vegfa* knockdown activity of the different miR-agshRNA combinations with or without intron embedment using co-transfection of a dual-luciferase reporter plasmid in HEK293 cells. Renilla luciferase (Rluc) fused to the *Vegfa* sequence is related to a firefly luciferase (Fluc) serving as internal control. All miR-agshRNA constructs were tested against a previously published triple-targeting miRNA-based cluster, miR(5,B,7). Rluc/Fluc ratio is the mean of triplicates normalized to the pcDNA3.1-CMV-intron control. Statistical comparisons were performed using one-way ANOVA followed by Tukey's post hoc test. CMV, cytomegalovirus promoter; poly(A), polyadenylation signal.

cellular toxicity.[20] However, these challenges may be circumvented by developments in RNAi technology. Notably, Ago2-dependent shRNAs (agshRNAs) mimicking miR451 biogenesis reduce the risk of off-target effects due to a lacking passenger strand,[21,22] and their independence from the dicer processing step and preference for Ago2-loading decrease the risk for oversaturation of the endogenous miRNA pathway.[23,24] To further increase therapeutic specificity agshRNA can be incorporated into a primary miRNA scaffold. This enables controlled and tissue-specific expression by using an RNA polymerase II (Pol II) promotor.[25] We have recently investigated the therapeutic potential of *VEGFA*-targeting microRNA-embedded agshRNAs (miR-agshRNAs). Retained *VEGFA* suppression as well as increased specificity compared with their canonical shRNA counterparts were demonstrated. In addition, a favorable safety profile including reduced endogenous miRNA pathway competition and increased cell viability was observed.[25–27] Furthermore, we have shown RPE-specific delivery and robust *Vegfa* suppression in the mouse eye after subretinal injection of a lentiviral (LV) vector encoding an expression cassette containing *Vegfa*-targeting miR-agshRNA driven by the RPE-specific VMD2 promotor.[26]

While these studies suggest the use of *VEGFA*-targeting miR-agshRNA as a viable strategy for anti-angiogenic gene therapy, the translational potential is optimally evaluated in an animal with ocular features more comparable with the human eye. A prominent example is the porcine eye, which has similar size and dimensions as well as important similarities in retinal anatomy. Indeed, CNV formation has been successfully modeled by laser induction in the porcine eye, suggesting it as a translational relevant model for ocular anti-angiogenic therapy.[28]

In this report, we thus explored the translational potential of dual *VEGFA*-targeting miR-agshRNAs in a porcine experimental CNV model.[28] Furthermore, we tested the transduction characteristics and retinal safety profile of single-stranded (ss) and self-complementary (sc) AAV2.8 encoding enhanced green fluorescent protein (GFP) in the porcine retina.

RESULTS

Potent *Vegfa* knockdown is obtained by combination and intron embedment of miR-agshRNAs

We designed pcDNA3.1-based expression vectors encoding our novel *Vegfa*-targeting miR-agshRNAs, targeting murine *Vegfa*, porcine *VEGFA*, and human *VEGFA*. Their ability to suppress *Vegfa* was initially established by comparing *in vitro* knockdown efficacy of various miR-agshRNA constructs. This was performed in dual luciferase co-transfection assays in HEK293 cells using a psiCHECK2-mVEGF reporter[25] with benchmarking to a miR-shRNA system, miR(5,B,7), previously validated *in vivo*.[29] miR(5,B,7) is based on the polycistronic miR106b cluster and modified to deliver three *Vegfa*-targeting shRNAs as part of an intron.[30] A series of cytomegalovirus (CMV)-driven miR-agshRNA constructs based on pcDNA3.1 were screened (Figure 1A). The previously published miR451-embedded agsh12 (miR451-12) and miR324-embedded agsh12 (miR324-12) constructs targeting *Vegfa* "target 12" were included.[25,26] In addition, two miR-agshRNA constructs (miR451-13 and miR324-13) targeting another previously identified potent *Vegfa* target site (designated "target 13") were included.[25]

All four constructs were tested using the target 12- and 13-sensitive psiCHECK2-mVEGF reporter[25] and compared with miR(5,B,7)

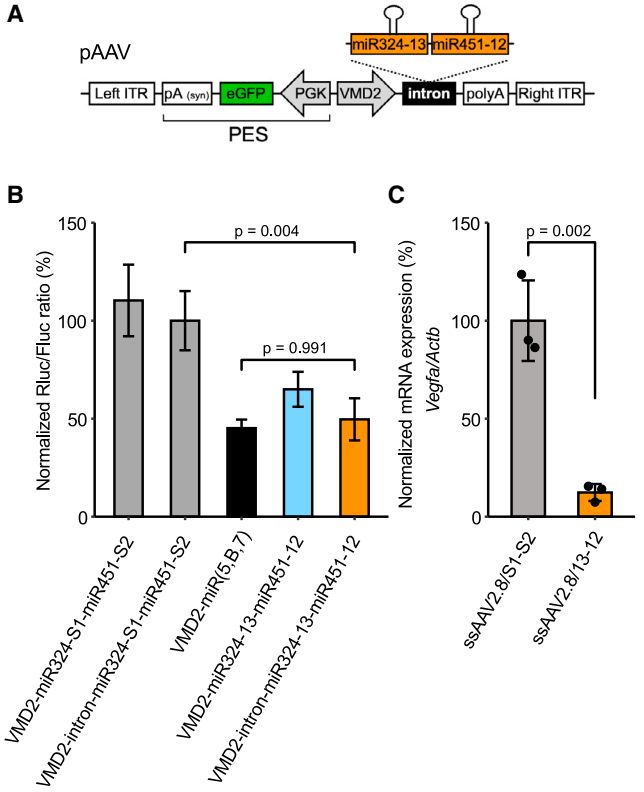

Figure 2. Design, *in vitro,* and *in vivo Vegfa* knockdown efficacy of VMD2-driven miR-agshRNA constructs

(A) Schematic presentation of the AAV2-based vector (pAAV) intron-miR324-13-miR451-12-PES, which expresses two miR-agshRNA units from the VMD2 promotor and GFP from a back-to-back PGK promoter. (B) Bar plot (mean ± SD) showing *Vegfa* knockdown efficacy of the pAAV-VMD2-intron-324-13-451-12-PES tested against a corresponding construct without intron embedment, two controls with irrelevant miR-agshRNAs and a pAAV with a previously published triple-targeting miRNA-based cluster (VMD2-miR(5,B,7)) estimated by dual luciferase co-transfection assay in human melanoma cells. Rluc/Fluc ratio is the mean of triplicates normalized to the pAAV-VMD2-intron-324-S1-451-S2 control. Statistical comparisons were performed using one-way ANOVA followed by Tukey's post hoc test. (C) Eight mice were injected in each group with 1×10^8 vg/eye of ssAAV2.8/13-12 or ssAAV2.8/S1-S2. From these eyes, three pools of GFP-positive cells were collected for RNA purification per group. RNA was purified from the GFP-positive pools, and *Vegfa* mRNA was quantified using RT-qPCR. Bar plot (mean ± SD) showing *Vegfa* mRNA expression relative to *Actb* and normalized to the ssAAV2.8/S1-S2-treated group. Each data point represents a pool of FACS-sorted GFP-positive murine RPE cells. Statistical comparison was performed using the Student's t test. eGFP, enhanced green fluorescent protein; ITR, inverted terminal repeat; PES, PGK-eGFP-Syn-pA.; PGK, phosphoglycerate kinase 1 promotor; poly(A), polyadenylation signal; Syn-pA, synthetic polyadenylation signal; VMD2, vitelliform macular dystrophy 2 promoter.

and an "empty" control. *Vegfa* knockdown was reported as reduced Renilla luciferase/Firefly luciferase ratios. miR451-12, miR451-13, miR324-12, and miR324-13 had knockdown efficacies of approximately 63%, 33%, 66%, and 47%, respectively (Figure 1B). However, none of the constructs could compete with the ∼85% knockdown achieved by miR(5,B,7) (Figure 1B).

Since miR(5,B,7) is based on a polycistronic miRNA cluster and targets the *Vegfa* transcript at three different sites,[29] we decided to explore the possibility of combining two miR-agshRNA units to achieve additive knockdown. These "double" miR-agshRNAs designated miR451-13-miR324-12 and miR324-13-miR451-12 differed only in the order of the miR scaffolds (Figure 1A). The double miR-agshRNAs provided a clear additive effect improving knockdown to 80% and 76% for miR451-13-miR324-12 and miR324-13-miR451-12, respectively (Figure 1B).

We have previously obtained enhanced miRNA expression from the miR106b cluster by placing it inside an intron.[31] Thus, we subsequently investigated whether intron embedment could improve *Vegfa* silencing. All single and double miR-agshRNA constructs were cloned into a pcDNA3.1-based plasmid equipped with a short β-globin exon-intron-exon fragment (for details see materials and methods). The dual luciferase assay revealed a tendency toward increased efficacy by intron embedding of these "spliceable" miR-agshRNAs (Figure 1B). The intron-miR324-13-miR451-12 produced a *Vegfa* knockdown of ∼87% resembling the knockdown achieved with miR(5,B,7).[29] Hence, the intron-miR324-13-miR451-12 construct was the most potent with significantly superior *Vegfa* knockdown compared with the best single miR-agshRNA construct (intron-miR451-12) ($p < 0.0001$).

VMD2-driven miR-agshRNAs induce robust *Vegfa* knockdown

The double miR-agshRNA system was then moved into an AAV2 transfer vector (pAAV2) modified from a vector previously used to induce robust silencing of *Vegfa* in a murine laser-induced CNV model.[29] This dual promoter AAV2 vector harbors a PGK-driven GFP reporter back-to-back with a VMD2-driven miR(5,B,7) and downstream AsRed reporter expression cassette.[32] The VMD2 promotor provides RPE-specific expression of miR(5,B,7) and AsRed. One of the two BGH polyadenylation signals was replaced with a shorter synthetic version (for details see materials and methods) and the miR(5,B,7)-AsRed unit was substituted with either miR324-13-miR451-12 or the corresponding intron-embedded version (Figure 2A). As non-targeting controls the *Vegfa*-targeting agshRNAs was substituted with hairpins designed to target HIV-1.[26] GFP reporter activity and intron-dependent enhancement of RNAi from the VMD2 promoter was evaluated in human-derived melanoma cells as the VMD2 promotor is active in these cells.[33] Highly significant reporter knockdown was observed for the VMD2-intron-miR324-13-miR451-12 construct (knockdown efficacy of ∼55%) compared with the corresponding HIV-targeting irrelevant control (S1/S2) ($p < 0.01$) (Figure 2B). No statistically significant difference was found between VMD2-intron-miR324-13-miR451-12 and the VMD2-driven miR(5,B,7) cluster (Figure 2B).

Finally, to assess expression and *in vivo Vegfa* knockdown of our VMD2-driven intron-miR324-13-miR451-12 construct, subretinal injections with 1×10^8 vg of ssAAV2.8/13-12 or

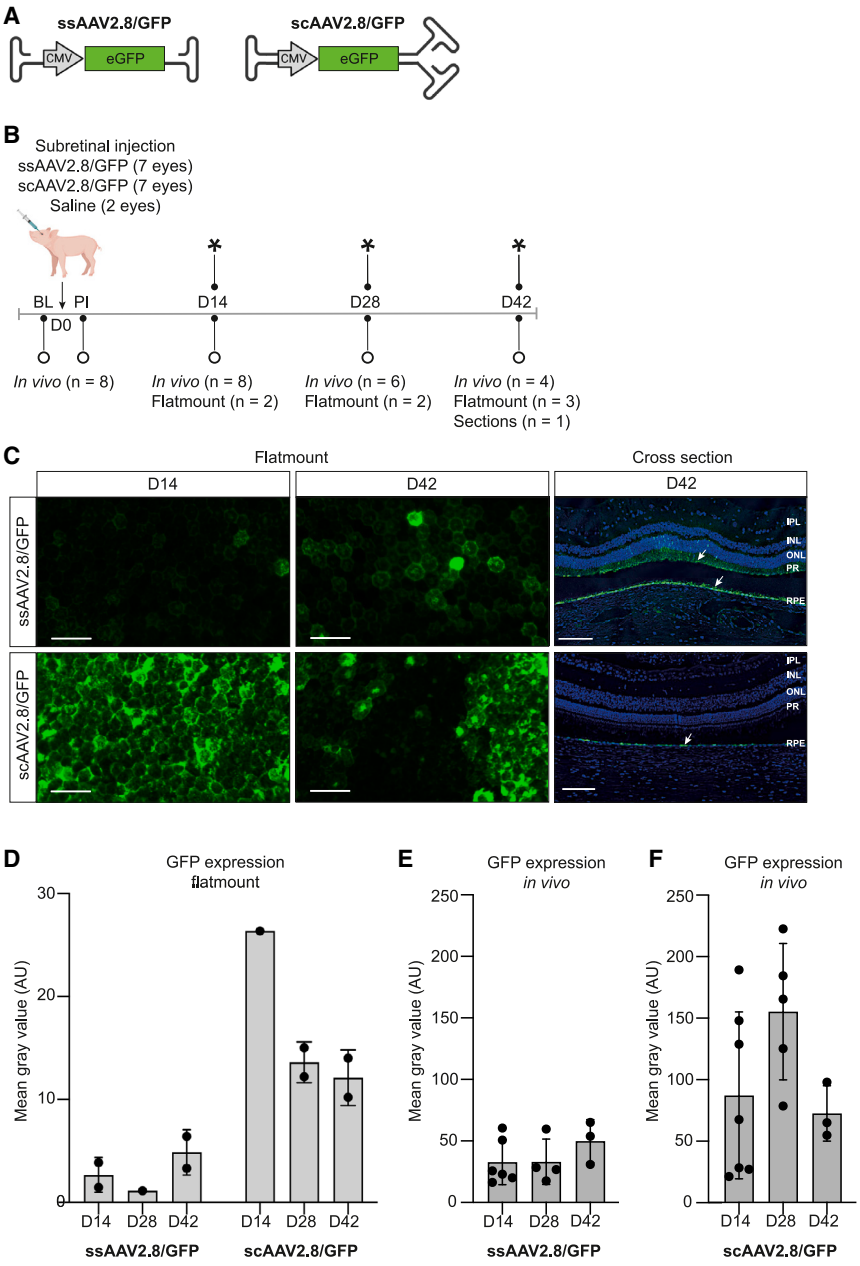

Figure 3. Transduction characteristics of ssAAV2.8/GFP and scAAV2.8/GFP in the porcine retina

(A) Schematic overview of ssAAV2.8 and scAAV2.8 encoding GFP driven by a CMV promotor. (B) Timeline of the delivery study showing the number (n) of animals injected with ssAAV2.8/GFP in one eye and scAAV2.8/GFP in the contralateral eye on D0 and at follow-ups on D14–D42. Black asterisks indicate clinical evaluation of ocular inflammation with slit lamp and fundus imaging. Circles indicate evaluation of GFP expression and retinal integrity using FI, FFI, and OCT *in vivo* and on RPE/choroidal flatmounts and retinal cross-sections. (C) Left and middle column: representative examples of RPE/choroidal flatmounts collected on D14 (left column) and D42 (middle column) after subretinal injection of ssAAV2.8/GFP (upper row) or scAAV2.8/GFP (lower row). GFP signal is presented in green. Scale bars, 50 μm. Right column: representative examples of retinal cross-sections from the injected area, obtained on D42 (right column) from eyes injected with ssAAV2.8/GFP (upper row) or scAAV2.8/GFP (lower row). DAPI staining (blue) and anti-GFP staining (green). White arrows point toward GFP expression. Scale bars, 100 μm. (D) Quantification of GFP expression on RPE/choroidal flatmounts obtained on D14, D28, and D42. Each dot represents one eye, n = 1–2. Data are plotted as mean ± SD. In two cases, only one eye was available for data analysis (scAAV2.8/GFP: D14; ssAVV2.8/GFP: D28). (E and F) Quantification of GFP signal by FFI on D14, D28, and D42. Each dot represents one eye, n = 3–7. Data are plotted as mean ± SD. In total, eight animals (P1–P8) were used in the delivery study. One eye (P3) was excluded. FFI settings: scAAV2.8/GFP (gain = 24 dB; flash level, 32 Ws), ssAAV2.8/GFP (gain = 24 dB; flash-level, 63 Ws). AAV, adeno-associated virus; AU, arbitrary units; BL, baseline; CMV, cytomegalovirus promoter; D0–D42, days 0–42; FI, fundus imaging; FFI, fundus fluorescence imaging; GFP, green fluorescent protein; INL, inner nuclear layer; IPL, inner plexiform layer; n, number of animals; OCT, optical coherence tomography; ONL, outer nuclear layer; PI, post-injection; PR, photoreceptor; RPE, retinal pigment epithelium; sc, self-complementary; ss, single-stranded.

ssAAV2.8/S1-S2 were performed in mice. The recombinant AAV vectors were based on AAV2 inverted terminal repeats (ITRs) and cross-packaged with the serotype 8 capsid. Seven weeks after subretinal injections with ssAAV2.8/13-12 or ssAAV2.8/S1-S2, we isolated transduced GFP-positive RPE cells using fluorescence-activated cell sorting (FACS). This enables the detection of changes in *Vegfa* mRNA levels specifically in transduced RPE cells (Figure 2C).[26,34] *Vegfa* mRNA levels were reduced by approximately 88% in GFP-positive RPE cells from mice injected with ssAAV2.8/13-12 compared with GFP-positive RPE cells from mice injected with ssAAV2.8/S1-S2 ($p = 0.002$) (Figure 2C). Representative examples of fundus imaging (FI) and fundus fluorescence imaging (FFI) from injected eyes and gating strategy for FACS are shown in Figure S1.

Subretinal delivery of ssAAV2.8/GFP and scAAV2.8/GFP results in efficient transduction of porcine RPE cells

In contrast to ssAAVs, scAAVs are packaged with a double-stranded vector genome. This provides higher genomic stability leading to increased levels of transgene expression[35] without the requirement for second-strand synthesis. Thus, scAAVs facilitate higher transduction efficiency and earlier onset of transgene expression.[36,37]

Table 1. Onset and duration of GFP expression after subretinal delivery of ssAAV2.8/GFP and scAAV2.8/GFP

			GFP *in vivo*			GFP flatmounts	
Animal	Eye	Treatment	D14	D28	D42	Time point	GFP signal
P1	OD	ssAAV2.8/GFP	yes	–	–	D14	yes
	OS	scAAV2.8/GFP	yes	–	–	–	–
P2	OD	scAAV2.8/GFP	yes	–	–	D14	yes
	OS	ssAAV2.8/GFP	no	–	–	D14	yes
P3	OD	scAAV2.8/GFP	yes	yes	–	D28	yes
	OS	excluded	–	–	–	–	–
P4	OD	ssAAV2.8/GFP	no	no	–	D28	yes
	OS	scAAV2.8/GFP	yes	yes	–	D28	yes
P5	OD	saline	no	no	no	–	–
	OS	saline	no	no	no	–	–
P6	OD	ssAAV2.8/GFP	yes	yes	yes	D42	yes
	OS	scAAV2.8/GFP	yes	yes	yes	D42	yes
P7	OD	scAAV2.8/GFP	yes	yes	yes	–	–
	OS	ssAAV2.8/GFP	yes	yes	yes	–	–
P8	OD	ssAAV2.8/GFP	no	yes	yes	D42	yes
	OS	scAAV2.8/GFP	yes	yes	yes	D42	Yes

(–) indicates eyes and time points where data are not available due to sacrifice of the experimental animal; AAV, adeno-associated virus; D14–42, days 14–42; GFP, green fluorescent protein; OD, oculus dexter; OS, oculus sinister; P1–P8, pigs 1–8; sc, self-complementary; ss, single-stranded.

However, ssAAV and scAAV vectors have not been compared in the porcine eye. We thus compared their transduction characteristics in a delivery study and assessed potential vector-related ocular inflammation and retinal toxicity. ssAAV and scAAV encoding GFP driven by a CMV promotor (Figure 3A) were used. Recombinant AAV vectors based on AAV2 ITR and cross-packaged with the serotype 8 capsid (ssAAV2.8/GFP and scAAV2.8/GFP) were used to efficiently transduce the RPE.[38]

At initiation of the experiment (day 0 [D0]), seven animals received a subretinal injection of ssAAV2.8/GFP in one eye and scAAV2.8/GFP in the other eye (Figure 3B). In accordance with previous studies an initial dose of 1×10^{10} vg/eye was chosen.[38,39] One animal was injected with saline in both eyes and used as a negative control. The subretinal injection was successful in 15/16 eyes. In one case an RPE tear was induced by the injection (Figure S2). Successful retinal transduction evaluated *in vivo* by FFI was observed in 10/14 vector-injected eyes corresponding to 7/7, 5/5, and 3/3 of the scAAV2.8/GFP-injected eyes on D14, D28, and D42, respectively (Table 1). In the ssAAV2.8/GFP-injected eyes the corresponding numbers were 3/6, 2/4, and 3/3 (Table 1), even though the flash level was increased to the maximum.

GFP expression on RPE/choroidal flatmounts was detectable in all eyes and at all time points evaluated (Table 1) and effective transduction of RPE cells was observed for ssAAV2.8/GFP and scAAV2.8/GFP (Figure 3C). Histological analysis of retinal cross-sections from the bleb area obtained on D42 showed successful transduction of RPE cells in eyes injected with ssAAV2.8/GFP and scAAV2.8/GFP (Figure 3C). Notably, GFP expression in photoreceptor (PR) cells was observed in the ssAAV2.8/GFP-injected eye, while it was absent in the eye injected with scAAV2.8/GFP.

Subretinal delivery of ssAAV2.8/GFP and scAAV2.8/GFP results in different expression profiles regarding time of on-set, expression level, and duration in porcine eyes

In all eyes, the GFP-positive area correlated to the subretinal bleb from D0 (5/10 eyes) or was slightly extended (5/10 eyes) (Figure S3). In some eyes, a distinctive GFP signal was bordering an area with lower GFP expression. There was no difference between vector type or right and left eye regarding the location and size of the GFP-positive area (Figure S3).

Transduction profile evaluation on RPE/choroidal flatmounts revealed a faster onset of GFP expression that led to approximately five times higher intensities on D14 in eyes injected with scAAV2.8/GFP compared with eyes injected with ssAAV2.8/GFP (Figures 3C, 3D, and S4). The highest GFP expression level was observed on D14 in the scAAV2.8/GFP-injected eyes, after which it slowly decreased (Figures 3C, 3D, and S4). In contrast, the highest level of GFP expression was observed on D42 in ssAAV2.8/GFP-injected eyes (Figures 3C, 3D, and S4). Furthermore, in the eyes injected with scAAV2.8/GFP, a tendency of reduced or lacking GFP expression in parts of the transduced area was observed on D28 and D42 compared with D14 (Figures 3C and S4). As observed on RPE/choroidal flatmounts, the highest level of GFP expression was observed on D42 by FFI in the ssAAV2.8/GFP-injected eyes

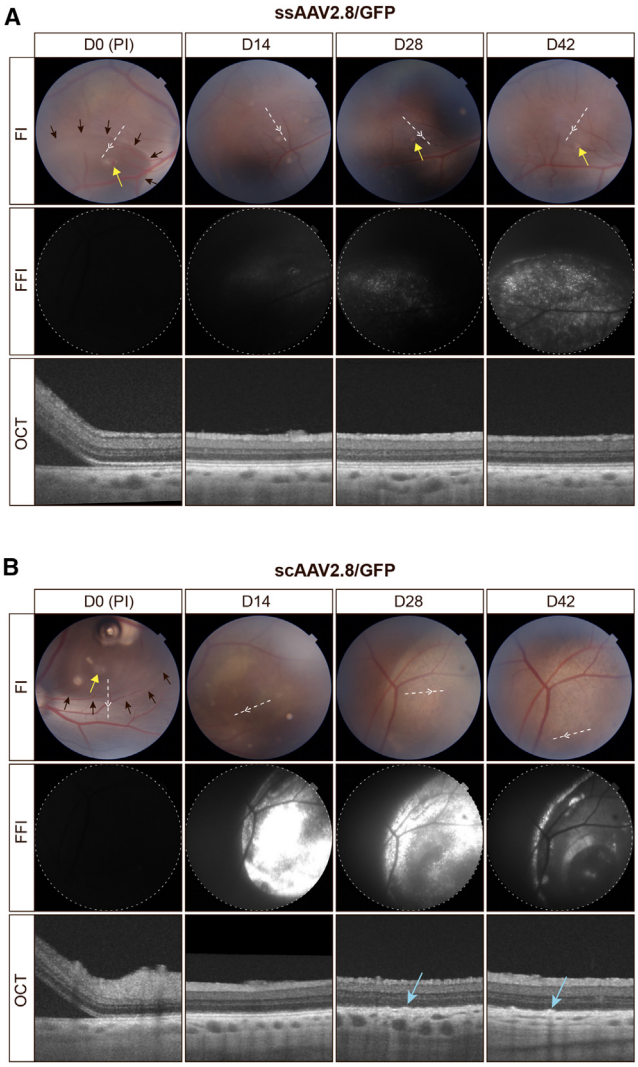

Figure 4. *In vivo* examination of the porcine retina post-injection of ssAAV2.8/GFP and scAAV2.8/GFP

Representative images of the porcine retina obtained with indicated imaging techniques on D0, D14, D28, and D42 after subretinal injection with ssAAV2.8/GFP (A) or scAAV2.8/GFP (B). FI (upper row) with black arrows indicating the border of the subretinal bleb on D0 and yellow arrows indicating the retinotomy and resulting scar tissue. Corresponding images obtained by FFI (middle row) showing GFP expression (white). Cross-sectional OCT scans (lower row) corresponding to the dashed line on FI. Light-blue arrowheads on OCT scans indicate hyperreflective irregularities adjacent to the RPE. FFI settings: scAAV2.8/GFP (gain = 24 dB; flash level = 32 Ws), ssAAV2.8/GFP (gain = 24 dB; flash level = 63 Ws). FI, fundus imaging; FFI, fundus fluorescence imaging; GFP, green fluorescent protein; OCT, optical coherence tomography; PI, post-injection.

(Figure 3E). However, the highest level of GFP expression was observed on D28 rather than on D14 in scAAV2.8/GFP-injected eyes (Figure 3F). Parallel to the observations on RPE/choroidal flatmounts, regions with reduced or lacking GFP expression on D28 and D42 compared with D14 were observed in eyes injected with scAAV2.8/GFP. These areas seem to correlate with areas showing high GFP expression on D14 (Figure S3). A similar pattern was observed in a single eye injected with ssAAV2.8/GFP, in which the area of high GFP expression on D14 was diminished on D42 (P6,OD) (Figure S3).

Self-complementary AAV2.8/GFP causes structural retinal changes in porcine eyes at the applied dose

The potential immune response to AAV vector particles is dose dependent and may be induced by the capsid, the vector DNA, or the transgene resulting in irreversible damage to the retinal tissue and/or a decrease of therapeutic efficacy due to neutralization of cells expressing the transgene.[38] Ocular inflammation following gene therapy, i.e., gene therapy-associated uveitis, can manifest as anterior chamber inflammation, vitritis, or retinitis.[38] Such inflammatory changes were evaluated using slit lamp examination and fundoscopy and graded according to the standardization of uveitis nomenclature at baseline, D14, D28, and D42 (Figure 3B). Assessment of RPE and retinal integrity was conducted with FI and cross-sectional optical coherence tomography (OCT) scans at the same time points (Figure 4). Encouragingly, we did not see clinical signs of intra-ocular inflammation in any of the eyes during the study. FI and OCT images at baseline revealed normal retinas for all animals with discrete variations of retinal pigmentation observed among the experimental animals similar to our previous study.[40] However, from D14 and onwards most eyes injected with scAAV2.8/GFP displayed pigmentary changes on FI (D14 = 43%; D28 = 80%; D42 = 100% of the eyes) (Figures 5A and 5B). Additional observations on OCT scans included the loss of distinct layering of the RPE/PR complex (D14 = 29%; D28 = 100%; D42 = 100% of the eyes), hyperreflective irregularities adjacent to the RPE (D28 = 80%; D42 = 100% of the eyes), and a single case (P1, OS, D14) of sparse cells in the vitreous body (Figures 4B, 5A, 5B, and S5; Table S1). In contrast, loss of distinct layering of the RPE/PR complex was only seen in a single ssAAV2.8/GFP-injected eye. This was restricted to a small region of the injection area corresponding to the area with the most intense GFP signal. No other structural changes were noted in eyes injected with ssAAV2.8/GFP.

In some transduced areas in the scAAV2.8/GFP-injected eyes, severe outer retinal alterations with complete loss of the ellipsoid and interdigitation zone were seen. These were sometimes accompanied by gross thinning of the outer nuclear layer (Figure S5). However, no general reduction in thickness was apparent in the transduced areas. Corresponding to areas of reduced *in vivo* GFP expression with accompanying disturbances of the RPE/PR complex in scAAV2.8/GFP-injected eyes, the RPE mosaic appeared disorganized with pleomorphism and polymegathism (Figure S6). In contrast, the RPE mosaic was well preserved in the GFP-positive areas of flatmounts from ssAAV2.8/GFP-injected eyes (Figure S6). Hematoxylin and eosin (H&E)-stained retinal cross-sections from one animal revealed preserved retinal layering and a continuous RPE layer in the GFP-positive and GFP-negative areas in both the ssAAV2.8/GFP- and scAAV2.8/GFP-injected eye (Figure 5C). However, the RPE layer appeared flattened with loss of pigment granules in the GFP-positive area of the scAAV2.8/GFP-injected eye (Figure 5C). In these areas,

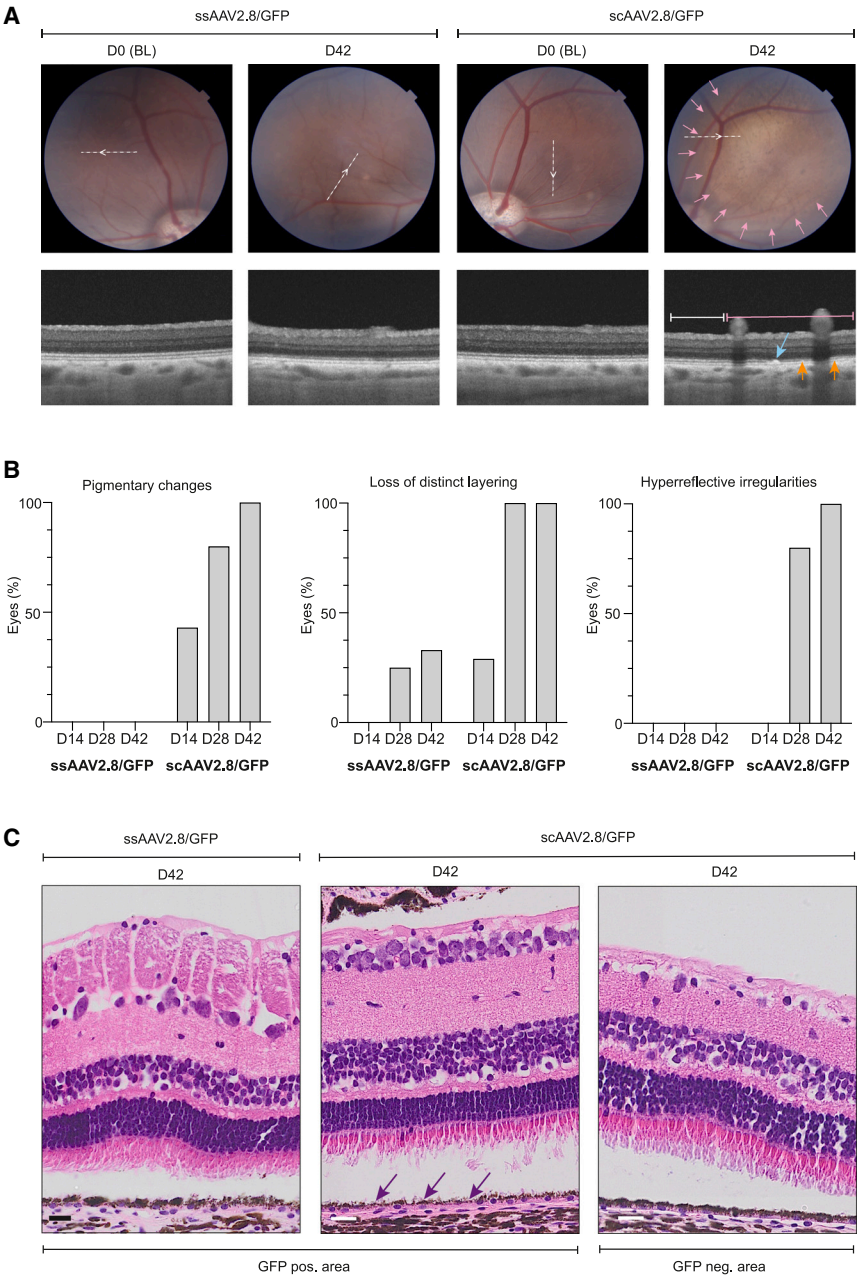

Figure 5. Structural retinal changes after injection with scAAV2.8/GFP

(A) Representative examples of FI (upper row) at baseline and on D42 after injection with ssAAV2.8/GFP or scAAV2.8/GFP. Light-pink arrows delimit the area of pigmentary changes. Cross-sectional OCT scan (lower row) corresponding to dashed white line on FI. White line indicates area outside the pigmentary changes, light-pink line indicates area with pigmentary changes. Light-blue arrow indicates hyperreflective irregularities adjacent to the RPE. Orange arrows point toward an area with loss of distinct layering of the RPE/PR complex. (B) Evaluation of structural retinal changes at different time points after subretinal injection of ssAAV2.8/GFP or scAAV2.8/GFP: Pigmentary changes (left), loss of distinct layering of the RPE/PR complex (middle), and hyperreflective irregularities adjacent to the RPE (right). Data are presented as percent of eyes available at the respective time point. ssAAV2.8/GFP (D14: n = 6; D28: n = 4; D42: n = 3); scAAV2.8/GFP (D14: n = 7, D28: n = 5; D42: n = 3). (C) H&E stains of retinal cross-section of the same eyes displayed in (A) injected with ssAAV2.8/GFP (GFP-positive area) or with scAAV2.8/GFP (GFP-positive and GFP-negative areas). Purple arrows point toward RPE cells with reduced pigment granules. Scale bars, 20 μm. BL, baseline; GFP, green fluorescent protein.

the PR outer segments also appeared blunted. No chorioretinal inflammatory infiltrates were present, and no difference in the distribution of the microglia and macrophage marker ionized calcium-binding adaptor molecule 1 (Iba1) was noticed in retinal cross-sections from the ssAAV2.8/GFP- and scAAV2.8/GFP-injected eye on D42 (Figure S7A).[41] Furthermore, no difference was observed in the GFP-positive and GFP-negative areas in scAA2.8/GFP-injected eyes (Figure S7A). Staining for glial fibrillary acidic protein (GFAP) in retinal cross-sections did not reveal Müller cell gliosis in eyes injected with either of the two AAV2.8/GFP vectors on D42 (Figure S7B).

In summary, we showed efficient transduction of RPE cells in the porcine retina for both ssAAV2.8/GFP and scAAV2.8/GFP. The latter showed faster onset of GFP expression but resulted in structural retinal changes that provide a serious concern for translational application. Thus, we proceeded with the ssAAV2.8 vector in the subsequent therapeutic *in vivo* study, although the changes most likely are related to a higher transgene expression level rather than the specific nature of the vector.

AAV-mediated subretinal delivery of *VEGFA*-targeting miR-agshRNA reduces CNV in a porcine model

Having established potent *Vegfa* knockdown with a miR-agshRNA construct *in vitro* and *in vivo* in mice, and shown successful ssAAV2.8-mediated gene transfer to the porcine RPE cells *in vivo*, we aimed to investigate the *in vivo* anti-angiogenic effect of the VMD2-driven intron-miR324-13-miR451-12 construct (Figure 2A). For this purpose the construct was packaged in a serotype 8 capsid with a single-stranded genome configuration (ssAAV2.8/13-12) and tested in a porcine laser-induced CNV model.[40] To increase efficacy and to account for a potentially weaker transgene expression by the VMD2 promotor compared with the CMV promotor[42] a slightly higher dose (3×10^{10} vg/eye) than in the delivery study was chosen. On D0, 10 animals received a subretinal injection of ssAAV2.8/13-12

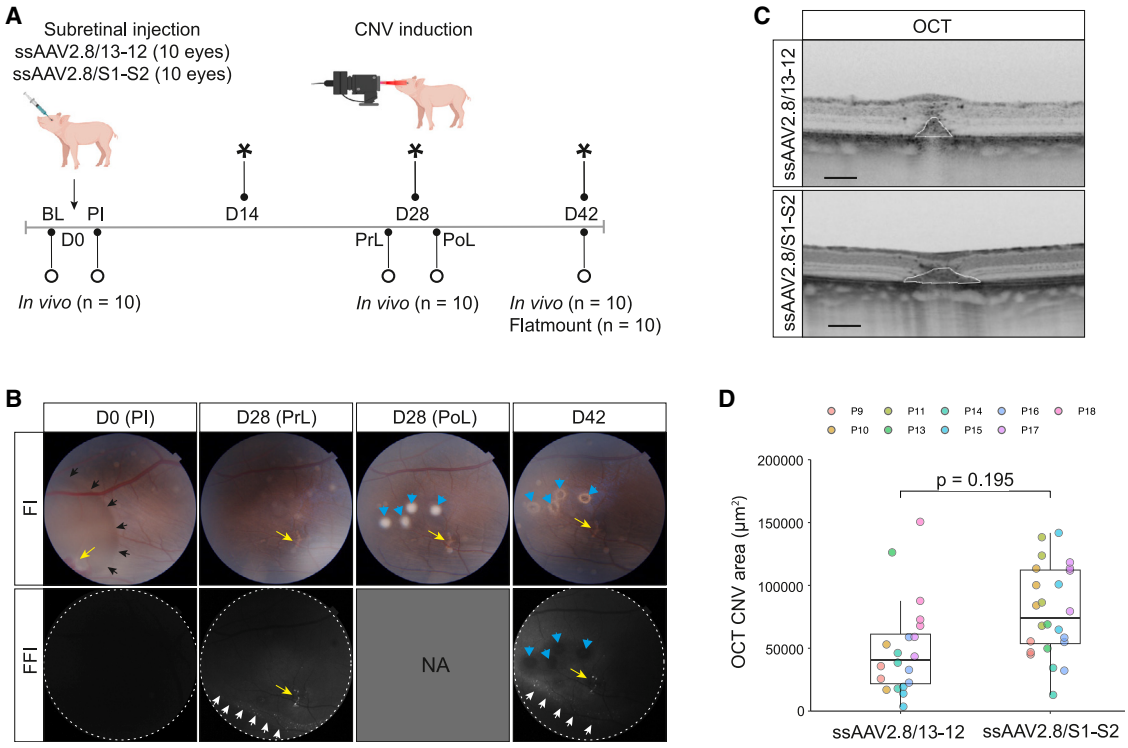

Figure 6. AAV-mediated subretinal delivery of *VEGFA*-targeting miR-agshRNA to the porcine retina

(A) Timeline of the intervention study, showing the number of animals for subretinal injection of ssAAV2.8/13-12 and ssAAV2.8/S1-S2 on D0, laser-mediated CNV induction on D28 and follow-ups on D14 and D42 post-injection. Black asterisks indicate clinical evaluation of ocular inflammation using slit lamp and fundus imaging. Circles indicate evaluation of GFP expression, retinal integrity, and CNV formation with FI, FFI, and OCT *in vivo* and on RPE/choroidal flatmounts. (B) Representative examples of FI (upper row) and corresponding FFI (lower row) of an eye injected with ssAAV2.8/S1-S2 on D0 (PI), pre- and post-laser treatment on D28 and D42. Yellow arrows point toward the retinotomy and resulting scar tissue. Black arrows indicate the border of the subretinal bleb on D0. Blue arrowheads indicate laser lesions on D28 and D42. GFP expression is shown in white on the images obtained by FFI, white arrows indicate the border of the GFP-positive area. (C). Representative examples of cross-sectional OCT scans (inverted colors) obtained on D42 showing subretinal CNV lesions (marked with a white border) for eyes injected with ssAAV2.8/13-12 (upper row) and ssAAV2.8/S1-S2 (lower row). Scale bars, 450 µm. (D) Analysis of CNV area on cross-sectional OCT scans for eyes injected with ssAAV2.8/13-12 and ssAAV2.8/S1-S2. Dot plot and boxplot of individual CNV measurements are presented. Statistical comparison was performed on mean CNV area per eye using the Wilcoxon rank-sum test. P9–P18 represents individual animals, n = 9. Both eyes in P12 were excluded. AAV, adeno-associated virus; BL, baseline; CNV, choroidal neovascularization; D0–D42, days 0–42; n, number of animals; NA, not available; OCT, optical coherence tomography; PI, post-injection; PoL, post-laser; PrL, pre-laser; ss, single-stranded.

in one eye and an irrelevant, non-targeting control (ssAAV2.8/S1-S2) in the other eye (Figure 6A).

On D28, varying levels of GFP expression were observed by FFI in 17/20 eyes. Intensities were in general lower than in the delivery study (Figures 6B and S8). In 3/20 eyes a brim of bright GFP expression surrounding an area with low GFP expression was present as seen in the delivery study (Figures 6B and S8). On D28, four laser burns were placed within the GFP-positive area or corresponding to the localization of the subretinal bleb observed on D0 if the GFP signal was indiscernible (Figure 6B). Inclusion/exclusion of lesions was based on predefined criteria (see materials and methods, Figures S9 and S10). In total, 44/80 lesions and 33/80 lesions were included in the *in vivo* and RPE/choroidal flatmount data analysis, respectively.

The anti-angiogenic effect of *VEGFA*-targeting miR-agshRNAs was evaluated on D42, i.e., 14 days after laser application. CNV size was evaluated *in vivo* on cross-sectional OCT scans (Figures 6B–6D) and on RPE/choroidal flatmounts stained with anti-cluster of differentiation 31 (CD31) and *Griffonia simplicifolia* type I lectin (GS-IB4) (Figures 7A–7C). As the most standardized method of quantifying CNVs, measurement of CNV areas on flatmounts constituted the primary outcome measure.[43] The OCT analysis showed a reduction in the mean cross-sectional CNV areas of eyes injected with ssAAV2.8/13-12 compared with eyes injected with ssAAV2.8/S1-S2 (Figures 6C and 6D). The median value was 36,540 μm^2 (interquartile range: 28,759 μm^2) and 79,310 μm^2 (interquartile range: 53,899 μm^2) in the ssAAV2.8/13-12- and ssAAV2.8/S1-S2-injected eyes, respectively. However, the difference did not reach statistical significance ($p = 0.195$). Notably, the mean CNV area measured on flatmounts was significantly reduced in eyes injected with ssAAV2.8/13-12 compared with eyes injected with ssAAV2.8/S1-S2 (Figure 7). This was true for quantification using the CD31 as well as the GS-IB4

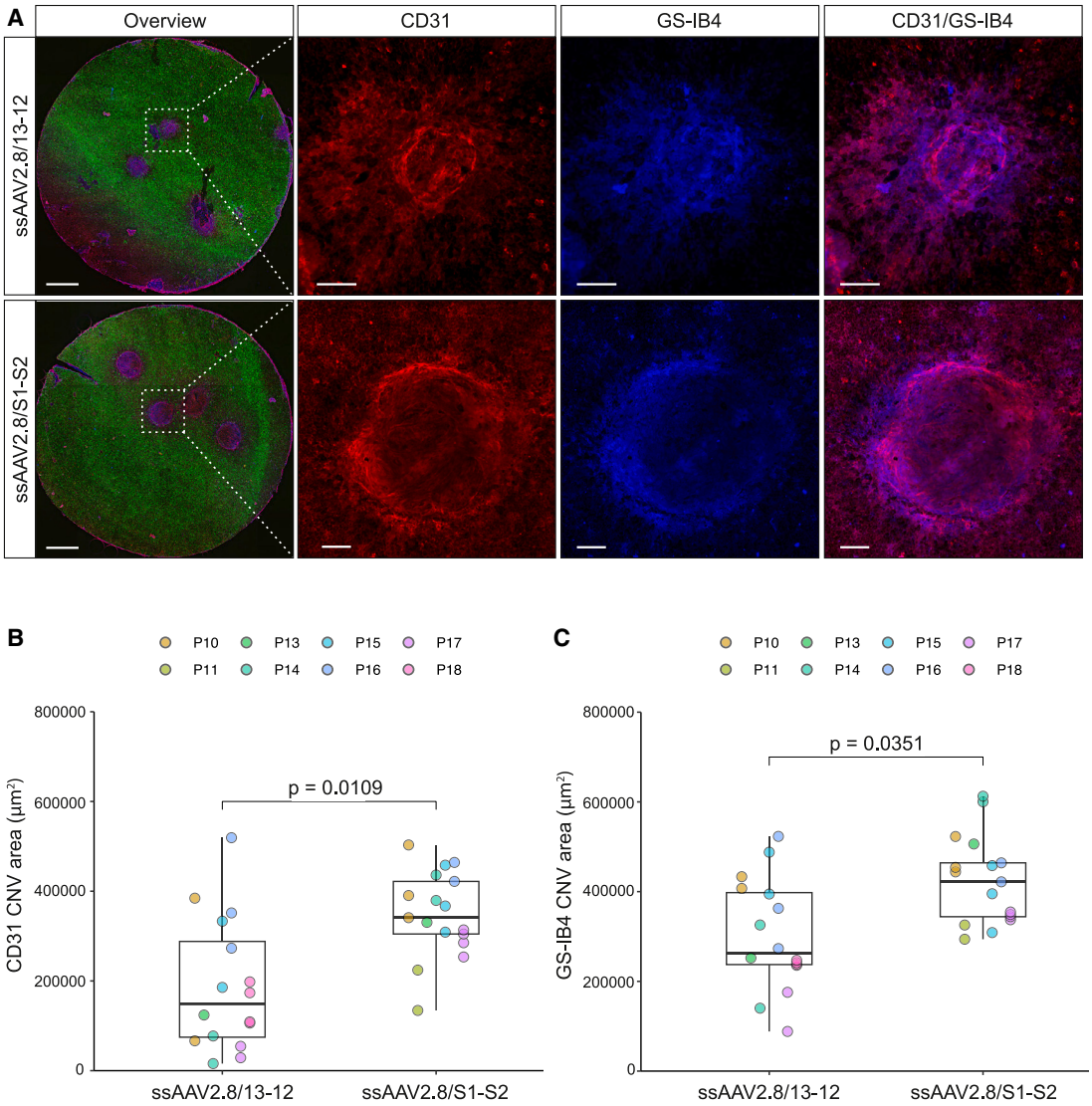

Figure 7. AAV-mediated subretinal delivery of *VEGFA*-targeting miR-agshRNA reduces CNV in a porcine model

(A) Representative examples of RPE/choroidal flatmounts from eyes harvested on D42 after injection of ssAAV2.8/13-12 (upper row) or ssAAV2.8/S1-S2 (lower row). Overview of the RPE/choroidal flatmounts. GFP expression (green), CD31 (red), GS-IB4 (blue). Scale bar, 800 µm (first column). Magnified images of CNV lesions corresponds to the white box in the first column. CD31 staining (red), GS-IB4 staining (blue) and CD31/GS-IB4 staining (fourth column). Scale bar, 100 µm. (B) Quantification of CD31 CNV area and (C) GS-IB4 CNV area from ssAAV2.8/13-12 and ssAAV2.8/S1-S2-injected eyes. Dot plot and boxplot of individual CNV measurements are presented. Statistical comparisons were performed on mean CNV area per eye using the Student's t test. P10–P18 represents individual animals, n = 8. Both eyes from P9 and P12 were excluded. AAV, adeno-associated virus; CD31, cluster of differentiation 31; CNV, choroidal neovascularization; GS-IB4, *Griffonia simplicifolia* type I lectin; ss, single-stranded.

signal: the mean CD31 CNV area was 175,008 ± 122,423 and 348,467 ± 91,057 µm^2 in the ssAAV2.8/13-12- and ssAAV2.8/S1-S2-injected eyes, respectively. The mean GS-IB4 CNV area was 300,780 ± 115,764 and 438,942 ± 101,456 µm^2 in the ssAAV2.8/13-12- and ssAAV2.8/S1-S2-injected eyes, respectively. The reduction using CD31 area amounted to 49.9% (13.8%; 86.0%) (p = 0.0109), while the reduction using GS-IB4 area amounted to 32.7% (2.7%; 62.6%) (p = 0.0351). Furthermore, as in the delivery study no clinical signs of intra-ocular inflammation were observed. Taken together, our data show that a *VEGFA*-targeting miR-agshRNA construct efficiently reduces CNV size in an experimental porcine model.

DISCUSSION

To our knowledge, this is the first study to evaluate the efficacy of AAV-based gene therapy delivering RNAi-therapeutics targeting *VEGFA* in a porcine CNV model, and the first to target *VEGFA* using novel agshRNA constructs in a large animal model. We have shown

that pol-II driven miR-agshRNA facilitate robust *Vegfa* knockdown *in vitro* and that the gene-silencing efficacy can be further increased by combining two *Vegfa*-targeting miR-agshRNAs in a single construct. Importantly, the potent *Vegfa* knockdown was validated *in vivo* in murine RPE cells and efficient reduction of CNV area was observed after subretinal delivery of ssAAV2.8 encoding *VEGFA*-targeting miR-agshRNA in the pig eye. Moreover, we are the first to compare transduction characteristics and retinal safety of ssAAV and scAAV vectors in the porcine retina.

We have previously demonstrated that a VMD2-driven, intron-embedded polycistronic miRNA cluster miR(5,B,7) expressing multiple *Vegfa*-targeting shRNAs successfully reduced *Vegfa* levels and CNV formation in a mouse model.[27,29,30] Furthermore, we have shown that our novel miR-agshRNA system provides advantages in terms of safety and specificity.[25,26] This study combines these approaches to pursue increased efficacy, specificity, and safety for translational application. Importantly, potent *in vitro Vegfa* knockdown and *in vivo* antiangiogenic effect were observed for an intron-embedded miR-agshRNA vector construct (intron-miR324-13-miR451-12) simultaneously expressing two *Vegfa*-targeting miR-agshRNAs (agshRNA-13 and agshRNA-12) known to mediate effective *Vegfa* knockdown individually.[25,26] Importantly, both the CMV-driven pcDNA3.1-based construct and the VMD2-driven pAAV2 construct showed *Vegfa* knockdown equal to their respective positive control (CMV- or VMD2-driven miR(5,B,7) cluster). We did not directly compare the knockdown efficacy of the CMV- and VMD2-driven constructs, but recent studies suggest a stronger transgene expression from universal promotors compared with RPE-specific promotors.[42] The observed knockdown efficacy and ability to combine miR-agshRNA constructs suggest vector-encoded RNAi therapeutics as an alternative strategy for anti-angiogenic ocular gene therapy. Notably, our novel agshRNA-platform, which is based on a small cassette expressing sequence-specific RNAi effectors, is easily packaged in AAV vectors and enables the combination of several RNAi effectors into a single vector construct. As RNAi enables specific targeting of any given transcribed gene due to its reliance on base pairing, these features allow simultaneous targeting of the multiple pathways leading to nAMD[26]— or other diseases in general. Thus, vector-delivered RNAi is a promising, versatile tool for the management of nAMD as well as other ocular and systemic conditions.[18]

The therapeutic potential of *VEGFA*-targeting miR-agshRNA was evaluated in a porcine laser-induced CNV model that has been experimentally validated.[40,43] Laser perforation of Bruch's membrane is an established method of CNV induction that has been amply used to evaluate anti-angiogenic therapies.[43] Most studies have been performed in rodents. However, our use of a large animal model offers several advantages. Notably, the comparable size and dimensions of the porcine and human eye enables the use of similar surgical methods and translation of pharmacokinetic properties. More similar anatomy and physiology also supports the translational value. In particular, the presence of central retinal specialization similar to the human macula should be noted.[44] Finally, the outbred nature may increase the external validity compared with inbred rodent models although it comes at a price of increased variation.[43] The validation of the therapeutic efficacy of *VEGFA*-targeting miR-agshRNA in this large animal model thus strongly confirms its translational potential.

In the therapeutic study, eyes were randomly assigned to treatment, and the investigators were blinded during surgery and analysis. Furthermore, inclusion/exclusion criteria were predefined. This randomized controlled design effectively reduces potential bias. Encouragingly, we observed a significant treatment effect on our primary outcome measure; CNV area evaluated on RPE/choroidal flatmounts. Although the effect estimate was associated with some variation, the best estimate of 30%–50% reduction in CNV size is a meaningful treatment effect. Importantly, the notable *Vegfa* knockdown in RPE cells from mice subjected to ssAAV2.8/13-12 injections validate that the therapeutic effect on CNV area corresponds with *VEGFA* inhibition.

Although not statistically significant, analysis of mean cross-sectional area on OCT scans also suggested an anti-angiogenic effect of our *VEGFA*-targeting miR-agshRNA construct. It should be noted that CNV quantification using OCT is less validated for preclinical CNV studies[28,43] with several potential sources of variation: The cross-sectional growth pattern of CNV membranes may differ from the growth pattern of the "en-face" area. Parts of the subretinal hyperreflective lesions may represent non-vascular scar tissue confounding CNV measurements. The delineation of the CNV membranes is challenged by laser-induced neuroretinal damage. In addition, the unpaired analysis not accounting for inter-eye correlation is expected to reduce statistical power.[45] As alternative strategies, optimization via another laser system[28] or protection of the neuroretina by subretinal injection of saline before laser application[40] could be explored.

Fluorescein angiography (FA) is commonly applied for the quantitative assessment of CNV membranes *in vivo*.[43] However, we did not use this method as the similar emission profiles of fluorescein (530 nm) and GFP (510 nm) were expected to cause spectral overlap. Further to this, FA still needs to be validated in porcine models of CNV.[28] Another attractive *in vivo* imaging alternative is OCT-angiography, which enables detection of vessel flow and thus detection of CNV membranes. OCT-angiography was performed in the present study, but the image quality was not sufficient for quantification of CNV size, mainly due to movement artifacts.

We also explored the differences in transduction characteristics and retinal safety of single-stranded and self-complementary AAV2.8 vectors in the porcine retina. The robust RPE transduction and GFP expression for both ssAAV2.8/GFP and scAAV2.8/GFP is consistent with a previous study by Mussolino et al., which showed effective transduction of both RPE and PR in the porcine retina by ssAAV2.8 vectors.[46] Surprisingly, PR transduction in retinal cross-sections was observed for ssAAV2.8/GFP, but not for scAAV2.8/GFP. However,

this finding may be explained by only evaluating retinal cross-sections on D42, where scAAV2.8-mediated transgene expression was decreased in some regions. The anti-GFP stains of the retinal cross-sections showed that the GFP-positive area correlated to the subretinal bleb from D0 or was slightly extended in all eyes. Notably, spreading to the sclera and choroid was not observed for any of the applied vectors.

A pattern of retinal GFP expression with a circular brim of strong GFP expression enclosing an area with weaker expression has been observed after subretinal delivery of GFP-encoding ssAAV2.8 vectors in non-human primates (NHPs).[47] Histologically these "halo-like" patterns corresponded to high and low GFP expression in the RPE. A dose dependency was suggested as the pattern could only be observed for doses of 1×10^{10} vg/eye and above. This observation should be considered in future studies as it indicates an undesirable variation in transgene expression across the bleb area.

Subretinal injection of scAAV2.8/GFP was associated with signs of toxicity, which included early reduction of transgene expression (from D28 and onwards) and structural retinal alterations. The nature of these structural alterations suggests cytotoxicity rather than functional transcriptional repression as the cause of reduced transgene expression. In previous studies, retinal toxicity and transgene inactivation has been related to cytotoxicity mediated by, e.g., transgene overexpression or immunotoxicity caused by a harmful immune response to the vector capsid, vector DNA, or transgene.[48] In some eyes, the areas of outer retinal alterations corresponded to areas with high GFP expression on D14. The fact that signs of toxicity were almost exclusively seen in scAAV2.8/GFP-injected eyes suggest a relation to high levels and/or fast onset of GFP expression.[49,50] Importantly, the absence of ocular inflammation throughout the study period does not support an immune-mediated mechanism. This was to be expected with the relatively low doses used in the delivery (1×10^{10} vg/eye) and intervention (3×10^{10} vg/eye) study. Indeed, an adverse ocular immune response following subretinal injection has mainly been observed with doses higher than 1×10^{11} vg/eye.[38,39]

In NHPs, signs of ocular inflammation have been detected using a dose of 1×10^{11} vg/eye. Inflammatory changes included the presence of anterior chamber cells peaking 3 days post-injection and the presence of vitreous cells from D7.[41] As our earliest clinical examination was conducted 14 days post-injection, initial signs of ocular inflammation may have been missed, but any persistent inflammation could be confidently excluded. The absence of an immune-mediated mechanism is further supported by the lack of difference in the number and localization of microglia in retinal sections between ssAAV2.8/GFP- and scAAV2.8/GFP-injected eyes. In conclusion, a cytotoxic effect of the transgene and *cis*-acting elements[51] seems most probable. However, detailed investigation into the underlying mechanism was challenged by the limited material for histopathological examination and other analyses as eyes were needed for evaluating GFP expression on flatmounts. Notably, delivery of our miR-agshRNA constructs in therapeutic doses did not cause similar alterations. This supports our previous observation of a favorable retinal safety profile of such constructs.[26]

It should be noted that our observations do not invalidate the use of scAAV for ocular gene therapy but rather suggest the importance of dose-titration. Indeed, one would also expect the observed changes to be seen with high doses of ssAAV2.8/GFP. Conversely, a reduction of the scAAV dose would be expected to provide a similar safety profile, while reaching the same levels of transgene expression as ssAAVs. Importantly, this reduction of vector dose could reduce the risk of an adverse immune response to, e.g., capsid antigens. In this context, but also to better understand the halo-like pattern, it would be of considerable clinical interest to perform dose escalation experiments with detailed examination of safety and expression profiles for different vector types in further studies. In addition, refined methods for dose selection based on, e.g., allometric scaling, would be advantageous.[52]

Our demonstration of *in vivo* anti-angiogenic effect of a *VEGFA*-targeting miR-agshRNA in a translational animal model combines two transformative technologies, gene therapy and RNAi. While the eye has been at the forefront of gene therapeutic development,[53] approved RNAi therapeutics are currently restricted to drugs with hepatic targeting. In addition, development of vector-delivered RNAi effectors are currently limited.[18] Thus, our investigation of an AAV-delivered therapeutic miR-agshRNA importantly contributes to the development of RNAi-based drugs for extra-hepatic disease and in particular vector-delivered RNAi that offers a unique possibility of long-term treatment of human disease. Specifically, our study firmly supports further clinical development of sustained anti-VEGFA RNAi therapeutics as a valuable treatment option for the management of nAMD. Besides offering safe and effective gene knockdown, the miR-agshRNA platform notably enables combination of several RNAi effectors into a single vector construct.[26] This allows simultaneous targeting of multiple pathways leading to nAMD, which may be necessary to address the complex pathogenesis of the disease.[13,53]

MATERIALS AND METHODS

Design of pcDNA3.1-based miR-agshRNA constructs

Construction of the "empty" pcDNA3.1-based plasmid vector, pcDNA3.1-CMV-MCS, as well as the miR451- and 324-embedded agsh12 (miR451-12 and miR324-12, respectively) has been described previously.[25,26] For this study, we similarly constructed miR451- and miR324-embedded agsh13 (miR451-13 and miR324-13, respectively), using synthetic DNA flanked by 5′ *SalI* and 3′ *XhoI* + *AgeI* sites (purchased as pUC57-based DNA from Genscript, Piscataway, NJ) and subcloning the *SalI-AgeI* fragment into the compatible *XhoI* and *AgeI* sites of pcDNA3.1-CMV-MCS. Double miR-agshRNA constructs were next created by opening the resulting miR451-13 and miR324-13 constructs using *XhoI* and *AgeI* and ligating the previously described miR451-12 or miR324-12 *XhoI-AgeI* fragments.[25]

Finally, we created spliceable versions of all the above constructs. This was done by inserting a custom-made exon-intron-exon unit (see Table S2, derived from the human β-globin gene) into the multiple cloning sites of pcDNA3.1-CMV-MCS. In short, a 330-base pair synthetic *SalI-XmaI* fragment (purchased as pUC57-based DNA from GenScript) holding the exon-intron-exon was subcloned into the compatible *XhoI* and *AgeI* sites of pcDNA3.1-CMV-MCS, creating the pcDNA3.1-CMV-intron. The pcDNA3.1-CMV-intron was used as recipient plasmid for all miR-agshRNA fragments as described above using *XhoI*, *EcoRI*, *AgeI* multiple cloning sites placed in the middle of the intron region. All plasmid constructs were validated by restriction enzyme digest and sequencing.

Design of the pAAV2-based RNAi transfer vectors

The previously published pAAV2-based transfer vector pAAV-VMD2-m5mBm7-asRED+PGK-eGFP-poly(A)[29] was modified by replacing one of the two BGH polyadenylation signals with a short synthetic poly(A) signal (see Table S2). In brief, the BGHpA unit downstream of GFP was removed by *BclI* and *ClaI* digest, and the synthetic poly(A) signal was inserted by oligo-mediated ligation of annealed and phosphorylated oligos with *BclI*- and *ClaI*-compatible ends. The resulting vector was termed pAAV-VMD2-mir(5,B,7)-asRED+PGK-eGFP-synpA. The double miR-agshRNA unit consisting of either miR324-13-miR451-12 or the non-targeting miR324-S1-miR451-S2 was PCR amplified using *BstBI*-tagged primers using pcDNA3.1-CMV-miR324-13-miR451-12 as template and cloned into the *BstBI* sites in pAAV-VMD2-mir(5,B,7)-asRED+PGK-eGFP-synpA. This effectively replaced the m5mBm7-asRED units with the double miR-agshRNA unit. Similarly, exon-binding *BstBI*-tagged primers were used to amplify inserts to create the pAAV-VMD2-intron-miR324-13-miR451-12+PGK-eGFP-synpA or the corresponding intron-miR324-S1-miR451-S2 version. PCR templates for the non-targeting miR324-S1-miR451-S2 control were prepared by insertion of miR451-S2 DNA flanked by *AgeI* sites (purchased as pUC57-based DNA from GenScript) into the existing pcDNA3.1-CMV-miR324-S1 construct[25] or a pcDNA3.1-CMV-intron-miR324-S1 derivative. All vector plasmids were validated by restriction enzyme digest and sequencing. PCR primers used to amplify miR-agshRNA units with or without intron embedment are shown in Table S2.

Cell culturing

All cell lines were kept in an incubator at 37°C and 5%, v/v, CO_2. HEK293 (CRL-1573; American Type Culture Collection, Manassas, VA) and human melanoma cell line[26] were cultured in T-75 cell culture flasks (Sarstedt, Nümbrecht, Germany) in Dulbecco's modified Eagle's medium (Sigma, Søborg, Denmark) supplemented with 10% fetal calf serum, 2 mM glutamine, 100 U/mL penicillin, and 0.1 mg/mL streptomycin.

Dual luciferase reporter assay

HEK293 cells were seeded at a density of 3,000 cells/well in white 96-well cell culture plates (Nunclon Delta surface, Thermo Scientific, Denmark). Twenty-four hours after seeding, cells were co-transfected using 34 ng vector DNA containing the RNAi effector and 6 ng psiCHECK2-based reporter, psiCHECK-mVEGF. miR-agshRNA expressing pcDNA3.1-based plasmids or a positive or negative control were used as RNAi effectors. The psiCHECK-mVEGF reporter contains target 12 and 13, which are orthologs in mouse and pig species as well as in humans.[25,26] Transfections were conducted using X-tremeGENE 9 (Roche, Basel, Switzerland) according to the manufacturer's protocol (DNA-to-transfection reagent ratio of 1 μg:7.5 μL). Forty-eight hours post-transfection, Rluc and Fluc expression levels were determined using the Dual-Glo Luciferase Assay System (Promega, Madison, WI) according to the manufacturer's protocol with a luminometer (MicroLuminat plus LB 96V, Berthold Technologies, Bad Wild-bad, Germany). Rluc/Fluc ratio was normalized to the negative control (pcDNA3.1-CMV-intron). Melanoma cells were seeded at a density of 110,000 cells/well in transparent standard flat-base 12-well cell culture plates (Sarstedt). Thirty hours after seeding, cells were co-transfected using 711 ng vector DNA containing the RNAi effector (the miR-agshRNA expressing pAAV2-based plasmid), or a positive or negative control, and 89 ng psiCHECK-mVEGF reporter. Transfections were conducted using JetPRIME (Polyplus-transfection, Illkirch, France) according to manufacturer's protocol (DNA-to-transfection reagent ratio of 1 μg:2.25 μL). The medium was changed 4 h post-transfection. Then, 42 h post-transfection, Rluc and Fluc expression levels were determined as described above; however, after lysis of cells, lysates were transferred to white 96-well plates (Nunclon Delta surface, Thermo Scientific). Three biological replicates were made for each experiment.

Vector production and preparation for subretinal injection

Single-stranded and self-complementary AAV vectors encapsulated in serotype 8 and containing the gene encoding GFP under the control of the CMV promoter (ssAAV2.8/GFP and scAAV2.8/GFP) were purchased from the in-stock selection of The University of North Carolina (UNC) Gene Therapy Center Vector Core (Chapel Hill, NC) for the delivery study with the following titers: ssAAV2.8/GFP: 7.9×10^{12} vg/mL; scAAV2.8/GFP: 4.0×10^{12} vg/mL. Prior to subretinal injection, AAV vectors were diluted in saline. Single-stranded AAV vectors for the intervention study were encapsulated in serotype 8 and produced at the UNC vector core using the following plasmids: pAAV-VMD2-intron-miR324-13-miR451-12+PGK-eGFP-synpA (therapeutic vector) and pAAV-VMD2-intron-miR324-S1-miR451-S2+PGK-eGFP-synpA (non-targeting control). The following titers were achieved: ssAAV2.8/13-12: 5.5×10^{12} vg/mL; ssAAV2.8/S1-S2: 2.2×10^{12} vg/mL. The purity of the ssAAV2.8/13-12 and ssAAV2.8/S1-S2 vectors was very high with full/empty ratios of 98% and 94%, respectively.[54]

Experimental animals

Mice

Animals were managed according to previously outlined procedures.[29] In brief, 8-week-old male C57BL/6JRj mice were procured from Janvier Labs (Le Genest-Saint-Isle, France) and maintained on a 12/12 h light/dark cycle at the Animal Facilities of the Department of Biomedicine, Aarhus University, Denmark, with unrestricted

access to water and Altromin maintenance feed (Altromin, Brogaarden, Denmark).

Pigs

Eighteen female, domestic pigs (crossing of Danish landrace [25%], Yorkshire [25%], Duroc [50%]), P1–18, aged 3 months with a weight of approximately 40 kg were used for the study. The animals used in this experiment were bred locally at a farm pig herd following Danish regulations. The animals were assigned to two studies: P1–P8 were part of the delivery study, which investigated transduction characteristics of ssAAV2.8/GFP and scAAV2.8/GFP (Figure 3); P9–P18 were part of the intervention study, exploring the therapeutic potential of *VEGFA*-targeting miR-agshRNA (Figures 6 and 7). Individual eyes were considered the experimental units. No formal power-calculation was performed due to unknown variance of the outcome measure. However, the number of experimental units were deemed sufficient to identify a relevant anti-angiogenic effect. The animals were kept in a stable with a light/dark cycle of 12 h/12 h at the Animal Facility, Department of Clinical Medicine, Aarhus University. The pigs were fed a normal finisher pig diet based on barley, wheat, and soy. Each pig was fed a rationed portion based on weight to limit the weight gain to between 2 and 4 kg per week. Hay and water were supplied *ad libitum*. The animals were kept in groups of 8 (delivery study) and 10 (intervention study). Before surgical intervention, animals were fasted overnight. During the first 2 days after surgical intervention (subretinal injection or CNV induction), the stable light was dimmed to prevent irritation of the injected eyes. Furthermore, regular inspection of the animals was performed by a veterinarian nurse. Animals were euthanized using an intravenous injection of 100 mg/kg pentobarbital (Euthanimal, 400 mg/mL; Scanvet, Fredensborg, Denmark).

The Animal Research: Reporting of In Vivo Experiments (ARRIVE) checklist for the porcine study is provided as supplemental information.

Anesthesia of the experimental animals

Mice

Before subretinal injection or *in vivo* fundoscopy, mice underwent anesthesia via intraperitoneal injection of ketamine and medetomidine hydrochloride (Ketador 60–100 mg/kg [Richter Pharma, Wels, Austria] and Cepetor 0.8–1.2 mg/kg [ScanVet Animal Health, Fredensborg, Denmark]). Pupils were dilated with a 1% tropicamide solution (Mydriacyl, Alcon Nordic, Copenhagen, Denmark) and eyes were lubricated with Carbomer eye gel (Visco-tears Alcon Nordic). Post procedures, mice were revived from anesthesia with atipamezole 0.5–1 mg/kg (Antisedan, Orion Pharma, Copenhagen, Denmark).

Pigs

Pre-anesthesia on D0 of both the delivery and the intervention study was achieved with an intramuscular injection of 1 mL/10 kg zoletil mix containing: tiletam and zolazepam (Zoletil 50 Vet; Virbac, Kolding, Denmark), xylazin (Rompun, 20 mg/mL; Bayer, Leverkusen, Germany), butorphanol (Butomidor Vet, 10 mg/mL; Salfarm, Kolding, Denmark), and ketamin (Ketaminol, 100 mg/mL; MSD Animal Health, Copenhagen, Denmark). General anesthesia was induced with 0.05–0.15 mg/kg propofol (10 mg/mL; Fresenius Kabi, Bad Homburg, Germany) intravenously, if required. Endotracheal intubation followed by artificial ventilation was conducted. General anesthesia was maintained with intravenous infusion of 3.5–6.5 mg/kg/h propofol and 15 μg/kg/h fentanyl (50 μg/mL; Hameln, Glostrup, Denmark). Both eyes were topically anesthetized using 0.4% oxybuprocaine eyedrops (minims Oxybuprocaine hydrochloride; Bausch & Lomb, Surrey, UK). Pupil were dilated with topical administration of 0.5% tropicamide eyedrops (minims Tropicamide 0.5%; Bausch & Lomb) and 10% metaoxedrin eyedrops (Metaoxedrin; Amgros, Copenhagen, Denmark). For follow-up examinations (D14, D28, D42) the pigs were anesthetized with an intramuscular injection of 1 mL/10 kg zoletil mix (see details above) and 0.5 mg/kg propofol (see details above) while connected to an oxygen mask (E-vet, Haderslev, Denmark) supplied with 100% oxygen.

Subretinal injection of AAV in mice

For the investigation of *Vegfa* knockdown in FACS-sorted RPE cells, 18 mice were subjected to bilateral subretinal injection with 1×10^8 vg of AAV in a total volume of 1 μL or 1 μL PBS. Injections were performed under a OPMI 1 FR PRO Surgical microscope (Zeiss, Jena, Germany). A 30-gauge needle was used to perforate the eye posterior to the limbus and a 35-gauge blunt-ended needle connected to a microinjection syringe with Silifilex tubing (World Precision Instruments, Sarasota, FL; NF35BL-2, NANOFIL, and SILFLEX-2) was then inserted through the opening and advanced through the vitreous cavity. The subretinal space was accessed by perforating the retina, and the AAV solution was then slowly injected. Eight mice received ssAAV2.8/13-12, eight mice ssAAV2.8/S1-S2, and two mice PBS with the type of injection being randomly assigned to the different cages, i.e., animals in a given cage received the same vector. The surgeon was not blinded.

Fundoscopic assessments were conducted using the Micron IV imaging system (Phoenix Research Laboratories, Pleasanton, CA) to detect GFP expression. At 4 weeks post-injection a fundoscopic examination was carried out and, 7 weeks post-injection the animals were sacrificed by cervical dislocation and the eyes were enucleated.

FACS of isolated murine RPE cells

RPE cells were gathered from ssAAV2.8/13-12-injected eyes (n = 15), ssAAV2.8/S1-S2-injected eyes (n = 16), and PBS-injected eyes (n = 4) as described previously (Figures S1A and S1B).[26,34] The eyes injected with AAV were further divided into groups of five or six eyes to obtain three pools of RPE cells for each vector construct. PBS injected eyes were pooled and used as negative control to set the gates for FACS sorting.

In summary, hyaluronidase was employed to detach the neural retina from the RPE layer, followed by trypsin enzymatic digestion combined with gentle shaking of the eyecup to detach RPE cells from Bruch's membrane. After centrifugation, RPE cells were suspended in FACS buffer (10 mM EDTA and 2% FCS in PBS), and the RPE

cell solution was passed through a 100-μm cell strainer (Thermo Fisher Scientific). The cells were maintained on ice and sorted immediately after collection.

FACS was conducted by the FACS Core Facility, Department of Biomedicine, Aarhus University, using the FACSAria III with 4 lasers (405, 488, 561, and 633 nm) and associated BD FACSDiva Software version 8.0.2 (BD Biosciences, San Jose, CA). The 488 nm laser was used for excitation, and 530/30 (eGFP detector) and 585/42 (PE detector) bandpass filters were used for detection. The cell population was identified based on forward scatter (FSC) and side scatter (SSC), where debris was removed. To avoid autofluorescent RPE cells, we identified the GFP-positive cell population based on fluorescence measured in the GFP and the neighboring PE detector (Figure S1C), as described previously.[34] Data were analyzed in FlowJo v10.8.1.

Purification of RNA from FACS-sorted murine RPE cells and cDNA synthesis

The collected cells were centrifuged at 240 × *g* for 15 min at 6°C and the cell pellets were used for RNA purification. RNA extraction was performed using the RNeasy Micro Kit (QIAGEN) following the manufacturer's protocol, with the exception that the gDNA eliminator column was omitted, and DNase treatment was not conducted on the column. QIAshredders (QIAGEN) were used for homogenization of cell lysates. RNA elution was carried out in a volume of 14 μL and treated with DNAfree (Thermo Fisher Scientific) according to the manufacturer's protocol. For the cDNA synthesis, 5 μL of the eluate was used in a 10 μL reaction using the iScript cDNA synthesis kit (Bio-Rad) according to the manufacturer's protocol.

RT-qPCR analyses of *Vegfa* in isolated murine RPE cells

Quantification of *Vegfa* mRNA transcripts in isolated murine RPE cells was performed according to established protocols.[26] In brief, RealQ Plus Master Mix Green (Ampliqon, Odense, Denmark) was prepared in a total reaction volume of 10 μL. A dose of 3 μL of the diluted (1:6) cDNA synthesis reaction was used as template. All reactions were analyzed in technical duplicates, except negative controls (-RT, UF H_2O). Fifty amplification cycles were used, but C_q values above 35 were not considered. The annealing temperature for both primer sets was 58°C, and the primer concentration was 0.5 μM. Standard curves were made using cDNA samples harvested from RPE cells from whole eyecups in 3-fold serial dilutions. PCR efficiency was 104% for *Vegfa* and 92% for *Actb*, which was used as a reference gene. The qPCR was performed using the LightCycler 480 II instrument (Roche). The range of C_q values was between 21.5 and 29.5 for *Atcb* and *Vegfa*. The -RT contamination controls indicated no DNA contamination with C_q values above 35. Concentrations were calculated from the C_q values using the standard curves. All primer sequences are available in Table S3.

Subretinal injection of AAV in pigs for delivery and intervention study

The subretinal injection procedure for the delivery and intervention studies only differed in the content of the injected AAV solution and is therefore described together (Figures S11A and S11B). The eyelids of the experimental animals were kept retracted using an eyelid speculum and corneas were frequently lubricated with topical administration of saline. The porcine retina was visualized with a surgical microscope (Opmi Lumera 300; Zeiss) in combination with a glass coverslip (16 mm diameter; Thermo Fisher Scientific, Roskilde, Denmark) separated from the cornea by a layer of Viscotears Eye Gel (2 mg/g; Alcon, Copenhagen, Denmark). Subretinal injections were performed in both eyes of all experimental animals. The sclera was incised nasally on the right eye (oculus dexter [OD]) and temporally on the left eye (oculus sinister [OS]) 4 mm from the corneal limbus using a surgical knife (Mani Ophthalmic Knife. MVR-Angled 21G; Mani, Takanezawa, Japan). A vitreo-retinal port system (23 gauge; DORC, Zuidland, the Netherlands) was introduced through the scleral incision. Subsequently, a subretinal cannula (Poly Tip Cannula 23/28 g × 2 mm tip; MedOne, Sarasota, FL) connected to an extension tube (5 cm, MedOne, Sarasota) and a 1-mL syringe containing the AAV solution was inserted in the port-system and slowly advanced toward the neuroretina. AAV solution (50 μL) was slowly injected subretinally in each eye.

In the delivery study, the two eyes of each pig were randomized to receive an AAV solution containing either 1×10^{10} vg ssAAV2.8/GFP or 1×10^{10} vg scAAV2.8/GFP. In the intervention study, the two eyes of each pig were randomized to receive an AAV solution containing either 3×10^{10} vg ssAAV2.8/13-12 or 3×10^{10} vg ssAAV2.8/S1-S2. In both studies, the retinal surgeon was blinded for the AAV solution given. After injection the subretinal cannula and port-system were removed and the pars plana incisions examined for leakage. None of the pars plana incisions required suturing. Chloramphenicol (1% chloramphenicol, Takeda Pharma, Vallensbæk Strand, Denmark) and ultracortenol (0,5% Agepha Pharma, Senec, Slovakia) ointment were applied to all eyes at the end of the surgery. Furthermore, the animal received an intramuscular injection of 0.4 mg/kg meloxicam (Metacam, 20 mg/mL; Boehringer Ingelheim Animal Health Nordics, Copenhagen, Denmark).

In vivo imaging

Immediately after the subretinal injection at baseline and on D14, D28, and D42 *in vivo* imaging (FI, FFI, and radial cross-sectional OCT scans) were obtained of the porcine retina using a modified multimodal retinal imaging device (deep range imaging OCT-1 Triton plus; Topcon, Roskilde, Denmark) as described previously.[40] In both studies, FI, FFI, and cross-sectional OCT scans centered on the injected area were acquired. Due to a stronger GFP expression signal in the eyes injected with scAAV2.8/GFP relative to ssAAV2.8/GFP, different FFI settings were used for imaging scAAV2.8/GFP (gain = 24 dB; flash level = 32 Ws) and ssAAV2.8/GFP (gain = 24 dB; flash level = 63 Ws) injected eyes. In the intervention study, cross-sectional OCT line-scans through the middle of the subretinal lesion were acquired to evaluate the size of the CNV area.

Evaluation of ocular inflammation

All pigs from both studies were examined for potential ocular inflammation on D14, D28, and D42 using slit lamp (Eyetec handheld slit lamp LED, LS-1B, MMC Optical, Rødovre, Denmark) and fundoscopy (Figure S11C). Anterior chamber cells and flare were graded by the standardization of uveitis nomenclature classification,[55] and vitreous haze was graded after Nussenblatt et al.[56]

CNV induction

In the intervention study, CNVs were induced by laser on D28 in all eyes. Prior to laser induction, images were obtained by FFI to assess GFP expression. Four burns, aimed to perforate Bruch's membrane, were placed in the area with positive GFP signal or corresponding to the bleb area on D0 if the GFP signal was absent. An IRIS medical Oculight SLx 810 nm laser (Iridex, Mountain View, CA) was used with the following parameters: spot size, 600 μm; power, 1000 mW; duration, 100 ms. The following criteria for inclusion and exclusion of the subretinal lesions were predefined (Figure S9): lesions were included if (1) the laser induction generated a focal spot with definitive whitening, (2) the lesion was placed within the bleb area (as seen by FI on D0) or within the area of GFP expression (determined by assessment of RPE/choroidal flatmounts), and (3) neovascularization was evident on immunostained RPE/choroidal flatmounts on D42. Choroidal hemorrhage caused by the laser induction, retinal trauma, or extensive retinal degeneration led to exclusion of the eye.

Harvest of tissue

Eyes were enucleated and transferred to a Petri dish (Thermo Fischer Scientific) with a circular filter paper (Frisenette, Knebel, Denmark) moistened with PBS (Dulbecco's phosphate buffered saline without magnesium and calcium; BioWest, Nuaillé, France). Remaining muscle and connective tissue were removed from the eye. A frontal cut was then made just posterior to the ora serrata to remove the anterior part including the cornea and lens. The remaining posterior eyecup was placed in 4% paraformaldehyde (Histolab Products, Askim, Sweden) solution and fixed for 1 h at room temperature (RT). Subsequently, the eyes were used to produce either RPE/choroidal flatmounts (P1–P6, P8, P9–P18) or retinal cross-sections (P7) for further analysis.

Preparation and immunostaining of RPE/choroidal flatmounts

Eyes were washed in PBS (BioWest) and dissected under a dissection microscope. Three to four incisions were made from the edges of the eyecups toward the optic nerve. In all eyes, the bleb area and/or the laser-induced subretinal lesions were identified under the dissection microscope aided by the fundus images obtained on D42. A 6-mm biopsy punch (Kai Europa, Solingen, Germany) was used to punch out the identified area. The neuroretina was gently removed and the RPE/choroid was separated from the sclera by careful dissection using a pair of Dumont style 3C Dumoxel tweezers (Sigma) and a pair of Vannas scissors (Simonsen & Weel, Vallensbæk Strand, Denmark).

Flatmounts from the intervention study were directly transferred to a Superfrost Plus glass slide (Menzel-Glaser, Braunschweig, Germany) with the RPE layer facing upwards. Remaining PBS was removed with filter paper. LifterSlip premium printed cover glasses (Erie Scientific Company, Portsmouth, NH) were mounted using Fluoromount-G Mounting Medium (Thermo Fisher Scientific).

Flatmounts from the intervention study were transferred to 48-well-plates containing 200 μL of permeabilization-blocking buffer (PBB; 4% BSA [VWR, Søborg, Denmark] and 0.5% Triton X-100 [Sigma] in PBS) and incubated for 2 h at 4°C on a rocking table. Subsequently, each sample was incubated with 150 μL primary antibody solution containing 1:100 diluted rat anti-CD31 antibody 0.5 mg/mL (557355, BD Pharmingen, San Diego, CA) and 1:100 diluted isolectin *Griffonia simplicifolia* (GS)-IB_4 biotin conjugate 1 mg/mL (I21414; Life Technologies, Nærum, Denmark) in PBB at 4°C overnight on a rocking table.

The next day flatmounts were washed in PBS-X (0.5% Triton in PBS) four times for 15 min at RT on a rocking table. Subsequently, samples were incubated with 150 μL secondary antibody solution containing 1:500 diluted goat anti-rat Alexa Fluor 568 2 mg/mL (ab175476; Abcam, Cambridge, UK) and 1:100 diluted streptavidin Alexa Fluor 405 conjugate 2 mg/mL (S32351; Thermo Fisher Scientific) in PBB in darkness for 2 h on a rocking table. Following washes in PBS-X, the flatmounts were mounted on Superfrost glass slides as described above.

Imaging and analysis of GFP expression and CNV size on RPE/choroidal flatmounts

RPE/choroidal flatmounts were imaged with an upright wide-field fluorescence microscope (Olympus VS120; Olympus, Tokyo, Japan) using identical settings. The images were obtained with a sensitive monochrome camera (Hamamatsu ORCA FLASH4.0V2; Hamamatsu, Japan) and associated VS-ASW imaging software. GFP expression on flatmounts from the delivery study was quantified on 20× magnification images using the ImageJ2 software (version 2.9.0/1.53t): The GFP expression area was identified and marked with the free-hand selection tool. The mean gray value of the defined area was then measured using the "analyze" function. The CNV area on RPE/choroidal flatmounts from the intervention study was similarly measured using the ImageJ2 software. The free-hand selection tool was used to define the area of CD31 and GS-IB_4 signal in the separate channels. Subsequently, areas were measured using the "analyze" function. Measurements were performed by one investigator blinded for the vector type injected.

Analysis of *in vivo* images

The CNV lesion area was evaluated on inverted images of the cross-sectional OCT scans, which had been acquired through the center of the lesions. The inverted images increased contrast thereby aiding identification of lesion borders. Measurements were performed by two investigators blinded for the vector type injected. Images were opened in the ImageJ2 software (version 2.9.0/1.53t) and the free-hand selection tool was used to define the inferior, lateral, and superior border of the lesion. The area was then measured with the

"analyze" tool in the software. GFP expression *in vivo* was evaluated on images obtained by FFI and the areas with GFP-positive signals defined and quantified as described above.

Preparation and immunostaining of retinal cross-sections

The eyecups from P7 (OD injected with scAAV2.8; OS injected with ssAAV2.8) were fixed in 4% paraformaldehyde (Histolab Products) solution and fixed for 1 h at RT. Identification of the bleb area was aided by fundus images from D0 and fundus fluorescence images from D42. The location was drawn on the outside of the eyecup. Paraffin embedding and sectioning were performed at the Department of Pathology, Aarhus University Hospital. Sections (4 μm) were cut from the identified bleb area and every sixth section was stained with H&E. The remaining sections were used for immunostaining with 4′,6-diamidino-2-phenylindole (DAPI) and anti-GFP, DAPI and anti-Iba1, or DAPI, anti-GFP, and anti-GFAP. After deparaffination in xylene (Merck, Søborg, Denmark) and rehydration with graded ethanol washes, the sections were placed in a jar with TE buffer pH 9.0 (10 mM Tris (Sigma 7–9; Sigma), 1 mM EDTA (Sigma) in H_2O) and heated in a microwave oven for 3.5 min on medium heat (for anti-GFP), 10 min on low heat (for anti-Iba1), and 10 min boiling in a jar with TE buffer (for anti-GFAP). Subsequently, the sections were placed on a rocking table to cool down for 30 min. Then, the sections were washed three times in PBS and blocked with a solution of 3% BSA (VWR) and 1% Triton X-100 (Sigma) in PBS. The slides were incubated with anti-GFP diluted 1:100 (G10362, 0.2 mg/mL, Invitrogen, MA), anti-Iba1 diluted 1:700 (019–19741, 0.5 mg/mL, Wako, Osaka, Japan), or anti-GFAP diluted 1:250 (sc-6170, 0.2 mg/mL, Santa Cruz Biotechnology, Dallas, TX) in a solution of 1% BSA and 1% Triton in PBS at 4°C in a humidity chamber overnight. On the next day, sections were warmed to RT, washed three times with PBS, and incubated with donkey anti-rabbit Alexa Fluor 568 (2 mg/mL) antibody diluted 1:400 in 1% BSA in PBS. After washing with PBS, sections were stained with DAPI (2 mg/mL, Sigma), rinsed twice with distilled water, dipped in ethanol, and dried. LifterSlip premium printed cover glasses (Erie Scientific) were applied using Fluoromount-G Mounting Medium (Thermo Fisher Scientific).

Statistics

Statistical analyses were performed using the R statistical software package, version R-4.2.2 (https://www.r-project.org/). Data are presented as mean ± SD unless otherwise stated. A significance level of $\alpha = 0.05$ was used and confidence intervals are presented accordingly. Data were assessed for normality by QQ plot inspection. Statistical differences between two group means were evaluated using a two-tailed Student's t test or non-parametrically using the Wilcoxon rank-sum test. Differences between multiple means were evaluated using one-way ANOVA followed by Tukey's post hoc test. Analysis of CNV measurements was performed using the mean lesion size per eye.

Study approval

The protocol was approved by the Danish animal Experiments Inspectorate (license number 2020-15-0201-00745 [mice] and 2018-15-0201-01518 [pigs]) and followed the Association for Research in Vision and Ophthalmology statement for use of animals in ophthalmic and vision research.

DATA AND CODE AVAILABILITY

All data are shown in the figure and supplemental information.

SUPPLEMENTAL INFORMATION

Supplemental information can be found online at https://doi.org/10.1016/j.omtm.2024.101242.

ACKNOWLEDGMENTS

The authors thank Tina Hindkjær and Helena Céline Kjær Byriel for expert technical assistance. Vitreoretinal surgeons Jesper Eriksen and Mette Slot Nielsen are thanked for valuable advice on the surgical procedures. Professor Jesper Hjortdal is thanked for lending surgical equipment. The AU Health Bioimaging Core Facility is thanked for the use of equipment and technical assistance. The Animal Facility, Department of Clinical Medicine, Aarhus University, is thanked for housing the pigs and providing the operational setting. The Animal Facility, Department of Biomedicine, Aarhus University, is thanked for housing the mice. FACS were performed at the FACS Core Facility, Department of Biomedicine, Aarhus University, Denmark, and the authors would like to thank the staff at the core facility for their support. This work was supported by the Faculty of Health Sciences, Aarhus University (PhD scholarships to B.K.F.-J., T.S.J., S.H.H., and A.B.L.), Fight for Sight, Denmark (to B.K.F.-J., T.S.J., and S.H.H.), Synoptik Foundation (to T.S.J. and S.H.H.), Maskinfabrikant Jochum Jensen og hustru Mette Marie Jensen F. Poulsens Mindelegat (to S.H.H.), Købmand Marie Kirstine Jensens Fonden, Danish Eye Research Foundation (to S.H.H.), APT Holding (to T.B. and T.J.C.), the Velux Foundation (grant no. 00038189 to T.J.C.), and the Independent Research Fund Denmark (grant no. 2034-00036B to T.J.C.). Figures were created using Biorender.com.

AUTHOR CONTRIBUTIONS

Writing – original draft, S.H.H., A.L.A., T.S.J., B.K.F.-J., L.A., and T.J.C.; writing – review & editing, S.H.H., A.L.A., B.K.F.-J., A.B.L., L.A., T.S.J., T.B., and T.J.C.; supervision, A.L.A., T.B., L.A., and T.J.C.; investigation, S.H.H., B.K.F.-J., A.B.L., T.S.J., R.L.A., T.J.C., and A.L.A.; methodology, S.H.H., B.K.F.-J., T.S.J., A.L.A., T.B., L.A., and T.J.C.

DECLARATION OF INTERESTS

The authors declare no competing interests.

REFERENCES

1. Coleman, H.R., Chan, C.C., Ferris, F.L., 3rd, and Chew, E.Y. (2008). Age-related macular degeneration. Lancet *372*, 1835–1845. https://doi.org/10.1016/s0140-6736(08)61759-6.

2. Rupert, R.A.B., Jost, B.J., Alain, M.B., Maria Vittoria, C., Aditi, D., Seth, R.F., David, S.F., Jill, E.K., John, H.K., Janet, L., et al. (2018). Prevalence and causes of vision loss in high-income countries and in Eastern and Central Europe in 2015: magnitude, temporal trends and projections. Br. J. Ophthalmol. *102*, 575–585. https://doi.org/10.1136/bjophthalmol-2017-311258.

3. Li, J.Q., Welchowski, T., Schmid, M., Mauschitz, M.M., Holz, F.G., and Finger, R.P. (2020). Prevalence and incidence of age-related macular degeneration in Europe: a systematic review and meta-analysis. Br. J. Ophthalmol. *104*, 1077–1084. https://doi.org/10.1136/bjophthalmol-2019-314422.

4. Rein, D.B., Wittenborn, J.S., Burke-Conte, Z., Gulia, R., Robalik, T., Ehrlich, J.R., Lundeen, E.A., and Flaxman, A.D. (2022). Prevalence of Age-Related Macular Degeneration in the US in 2019. JAMA Ophthalmol. *140*, 1202–1208. https://doi.org/10.1001/jamaophthalmol.2022.4401.

5. Fleckenstein, M., Keenan, T.D.L., Guymer, R.H., Chakravarthy, U., Schmitz-Valckenberg, S., Klaver, C.C., Wong, W.T., and Chew, E.Y. (2021). Age-related macular degeneration. Nat. Rev. Dis. Primers *7*, 31. https://doi.org/10.1038/s41572-021-00265-2.

6. Rubio, R.G., and Adamis, A.P. (2016). Ocular Angiogenesis: Vascular Endothelial Growth Factor and Other Factors. Dev. Ophthalmol. *55*, 28–37. https://doi.org/10.1159/000431129.

7. Lin, F.-L., Wang, P.-Y., Chuang, Y.-F., Wang, J.-H., Wong, V.H.Y., Bui, B.V., and Liu, G.-S. (2020). Gene Therapy Intervention in Neovascular Eye Disease: A Recent Update. Mol. Ther. *28*, 2120–2138. https://doi.org/10.1016/j.ymthe.2020.06.029.

8. Bek, T., and Bech, B.H. (2023). Visual acuity and causes of central visual loss in the adult Danish population 2020-2022. Results from the FORSYN study. Acta Ophthalmol. *101*, 504–513. https://doi.org/10.1111/aos.15641.

9. Rakoczy, E.P., Magno, A.L., Lai, C.M., Pierce, C.M., Degli-Esposti, M.A., Blumenkranz, M.S., and Constable, I.J. (2019). Three-Year Follow-Up of Phase 1 and 2a rAAV.sFLT-1 Subretinal Gene Therapy Trials for Exudative Age-Related Macular Degeneration. Am. J. Ophthalmol. *204*, 113–123. https://doi.org/10.1016/j.ajo.2019.03.006.

10. Constable, I.J., Pierce, C.M., Lai, C.M., Magno, A.L., Degli-Esposti, M.A., French, M.A., McAllister, I.L., Butler, S., Barone, S.B., Schwartz, S.D., et al. (2016). Phase 2a Randomized Clinical Trial: Safety and Post Hoc Analysis of Subretinal rAAV.sFLT-1 for Wet Age-related Macular Degeneration. EBioMedicine *14*, 168–175. https://doi.org/10.1016/j.ebiom.2016.11.016.

11. Grishanin, R., Vuillemenot, B., Sharma, P., Keravala, A., Greengard, J., Gelfman, C., Blumenkrantz, M., Lawrence, M., Hu, W., Kiss, S., and Gasmi, M. (2019). Preclinical Evaluation of ADVM-022, a Novel Gene Therapy Approach to Treating Wet Age-Related Macular Degeneration. Mol. Ther. *27*, 118–129.

12. Campochiaro, P.A., Avery, R., Brown, D.M., Heier, J.S., Ho, A.C., Huddleston, S.M., Jaffe, G.J., Khanani, A.M., Pakola, S., Pieramici, D.J., et al. (2024). Gene therapy for neovascular age-related macular degeneration by subretinal delivery of RGX-314: a phase 1/2a dose-escalation study. Lancet. https://doi.org/10.1016/S0140-6736(24)00310-6.

13. Askou, A.L., Jakobsen, T.S., and Corydon, T.J. (2023). Toward lentiviral vectors for antiangiogenic ocular gene therapy. Mol. Ther. Methods Clin. Dev. *30*, 443–446. https://doi.org/10.1016/j.omtm.2023.08.007.

14. Fire, A., Xu, S., Montgomery, M.K., Kostas, S.A., Driver, S.E., and Mello, C.C. (1998). Potent and specific genetic interference by double-stranded RNA in Caenorhabditis elegans. Nature *391*, 806–811. https://doi.org/10.1038/35888.

15. Elbashir, S.M., Harborth, J., Lendeckel, W., Yalcin, A., Weber, K., and Tuschl, T. (2001). Duplexes of 21-nucleotide RNAs mediate RNA interference in cultured mammalian cells. Nature *411*, 494–498. https://doi.org/10.1038/35078107.

16. Brummelkamp, T.R., Bernards, R., and Agami, R. (2002). A system for stable expression of short interfering RNAs in mammalian cells. Science *296*, 550–553. https://doi.org/10.1126/science.1068999.

17. Paddison, P.J., Caudy, A.A., Bernstein, E., Hannon, G.J., and Conklin, D.S. (2002). Short hairpin RNAs (shRNAs) induce sequence-specific silencing in mammalian cells. Genes Dev. *16*, 948–958. https://doi.org/10.1101/gad.981002.

18. Corydon, I.J., Fabian-Jessing, B.K., Jakobsen, T.S., Jørgensen, A.C., Jensen, E.G., Askou, A.L., Aagaard, L., and Corydon, T.J. (2023). 25 years of maturation: A systematic review of RNAi in the clinic. Mol. Ther. Nucleic Acids *33*, 469–482. https://doi.org/10.1016/j.omtn.2023.07.018.

19. Birmingham, A., Anderson, E.M., Reynolds, A., Ilsley-Tyree, D., Leake, D., Fedorov, Y., Baskerville, S., Maksimova, E., Robinson, K., Karpilow, J., et al. (2006). 3' UTR seed matches, but not overall identity, are associated with RNAi off-targets. Nat. Methods *3*, 199–204. https://doi.org/10.1038/nmeth854.

20. Grimm, D., Streetz, K.L., Jopling, C.L., Storm, T.A., Pandey, K., Davis, C.R., Marion, P., Salazar, F., and Kay, M.A. (2006). Fatality in mice due to oversaturation of cellular microRNA/short hairpin RNA pathways. Nature *441*, 537–541. https://doi.org/10.1038/nature04791.

21. Shang, R., Zhang, F., Xu, B., Xi, H., Zhang, X., Wang, W., and Wu, L. (2015). Ribozyme-enhanced single-stranded Ago2-processed interfering RNA triggers efficient gene silencing with fewer off-target effects. Nat. Commun. *6*, 8430. https://doi.org/10.1038/ncomms9430.

22. Liu, Y.P., Schopman, N.C.T., and Berkhout, B. (2013). Dicer-independent processing of short hairpin RNAs. Nucleic Acids Res. *41*, 3723–3733. https://doi.org/10.1093/nar/gkt036.

23. Ma, H., Zhang, J., and Wu, H. (2014). Designing Ago2-specific siRNA/shRNA to Avoid Competition with Endogenous miRNAs. Mol. Ther. Nucleic Acids *3*, e176. https://doi.org/10.1038/mtna.2014.27.

24. Harwig, A., Kruize, Z., Yang, Z., Restle, T., and Berkhout, B. (2017). Analysis of AgoshRNA maturation and loading into Ago2. PLoS One *12*, e0183269. https://doi.org/10.1371/journal.pone.0183269.

25. Kaadt, E., Alsing, S., Cecchi, C.R., Damgaard, C.K., Corydon, T.J., and Aagaard, L. (2019). Efficient Knockdown and Lack of Passenger Strand Activity by Dicer-Independent shRNAs Expressed from Pol II-Driven MicroRNA Scaffolds. Mol. Ther. Nucleic Acids *14*, 318–328. https://doi.org/10.1016/j.omtn.2018.11.013.

26. Alsing, S., Doktor, T.K., Askou, A.L., Jensen, E.G., Ahmadov, U., Kristensen, L.S., Andresen, B.S., Aagaard, L., and Corydon, T.J. (2022). VEGFA-targeting miRagshRNAs combine efficacy with specificity and safety for retinal gene therapy. Mol. Ther. Nucleic Acids *28*, 58–76. https://doi.org/10.1016/j.omtn.2022.02.019.

27. Becker, J., Fischer, N., and Grimm, D. (2022). Right on target: The next class of efficient, safe, and specific RNAi triggers. Mol. Ther. Nucleic Acids *28*, 363–365. https://doi.org/10.1016/j.omtn.2022.03.027.

28. Jakobsen, T.S., Fabian-Jessing, B.K., Hansen, S., Bek, T., Askou, A.L., and Corydon, T.J. (2023). Porcine models of choroidal neovascularization: A systematic review. Exp. Eye Res. *234*, 109590. https://doi.org/10.1016/j.exer.2023.109590.

29. Askou, A.L., Alsing, S., Benckendorff, J.N.E., Holmgaard, A., Mikkelsen, J.G., Aagaard, L., Bek, T., and Corydon, T.J. (2019). Suppression of Choroidal Neovascularization by AAV-Based Dual-Acting Antiangiogenic Gene Therapy. Mol. Ther. Nucleic Acids *16*, 38–50. https://doi.org/10.1016/j.omtn.2019.01.012.

30. Askou, A.L., Benckendorff, J.N.E., Holmgaard, A., Storm, T., Aagaard, L., Bek, T., Mikkelsen, J.G., and Corydon, T.J. (2017). Suppression of Choroidal Neovascularization in Mice by Subretinal Delivery of Multigenic Lentiviral Vectors Encoding Anti-Angiogenic MicroRNAs. Hum. Gene Ther. Methods *28*, 222–233. https://doi.org/10.1089/hgtb.2017.079.

31. Aagaard, L.A., Zhang, J., von Eije, K.J., Li, H., Saetrom, P., Amarzguioui, M., and Rossi, J.J. (2008). Engineering and optimization of the miR-106b cluster for ectopic expression of multiplexed anti-HIV RNAs. Gene Ther. *15*, 1536–1549. https://doi.org/10.1038/gt.2008.147.

32. Askou, A.L., Pournaras, J.A.C., Pihlmann, M., Svalgaard, J.D., Arsenijevic, Y., Kostic, C., Bek, T., Dagnaes-Hansen, F., Mikkelsen, J.G., Jensen, T.G., and Corydon, T.J. (2012). Reduction of choroidal neovascularization in mice by adeno-associated virus-delivered anti-vascular endothelial growth factor short hairpin RNA. J. Gene Med. *14*, 632–641. https://doi.org/10.1002/jgm.2678.

33. Askou, A.L., Aagaard, L., Kostic, C., Arsenijevic, Y., Hollensen, A.K., Bek, T., Jensen, T.G., Mikkelsen, J.G., and Corydon, T.J. (2015). Multigenic lentiviral vectors for combined and tissue-specific expression of miRNA- and protein-based antiangiogenic factors. Mol. Ther. Methods Clin. Dev. *2*, 14064. https://doi.org/10.1038/mtm.2014.64.

34. Alsing, S., Lindholm, A.B., Haldrup, J., Jensen, E.G., Mikkelsen, J.G., Aagaard, L., Askou, A.L., and Corydon, T. (2022). Simple autofluorescence-restrictive sorting of eGFP+ RPE cells allows reliable assessment of targeted retinal gene therapy. Front. Drug Deliv. *2*. https://doi.org/10.3389/fddev.2022.898568.

35. Natkunarajah, M., Trittibach, P., McIntosh, J., Duran, Y., Barker, S.E., Smith, A.J., Nathwani, A.C., and Ali, R.R. (2008). Assessment of ocular transduction using single-stranded and self-complementary recombinant adeno-associated virus serotype 2/8. Gene Ther. *15*, 463–467. https://doi.org/10.1038/sj.gt.3303074.

36. McCarty, D.M., Monahan, P.E., and Samulski, R.J. (2001). Self-complementary recombinant adeno-associated virus (scAAV) vectors promote efficient transduction independently of DNA synthesis. Gene Ther. *8*, 1248–1254. https://doi.org/10.1038/sj.gt.3301514.

37. Petersen-Jones, S.M., Bartoe, J.T., Fischer, A.J., Scott, M., Boye, S.L., Chiodo, V., and Hauswirth, W.W. (2009). AAV retinal transduction in a large animal model species: comparison of a self-complementary AAV2/5 with a single-stranded AAV2/5 vector. Mol. Vis. *15*, 1835–1842.

38. Bucher, K., Rodríguez-Bocanegra, E., Dauletbekov, D., and Fischer, M.D. (2021). Immune responses to retinal gene therapy using adeno-associated viral vectors - Implications for treatment success and safety. Prog. Retin. Eye Res. *83*, 100915. https://doi.org/10.1016/j.preteyeres.2020.100915.

39. Beltran, W.A., Boye, S.L., Boye, S.E., Chiodo, V.A., Lewin, A.S., Hauswirth, W.W., and Aguirre, G.D. (2010). rAAV2/5 gene-targeting to rods:dose-dependent efficiency and complications associated with different promoters. Gene Ther. *17*, 1162–1174. https://doi.org/10.1038/gt.2010.56.

40. Hansen, S., Askou, A.L., la Cour, M., Corydon, T.J., and Bek, T. (2021). Subretinal Saline Protects the Neuroretina From Thermic Damage During Laser Induction of Experimental Choroidal Neovascularization in Pigs. TVST *10*, 29. https://doi.org/10.1167/tvst.10.7.29.

41. Reichel, F.F., Dauletbekov, D.L., Klein, R., Peters, T., Ochakovski, G.A., Seitz, I.P., Wilhelm, B., Ueffing, M., Biel, M., Wissinger, B., et al. (2017). AAV8 Can Induce Innate and Adaptive Immune Response in the Primate Eye. Mol. Ther. *25*, 2648–2660. https://doi.org/10.1016/j.ymthe.2017.08.018.

42. Johari, Y.B., Mercer, A.C., Liu, Y., Brown, A.J., and James, D.C. (2021). Design of synthetic promoters for controlled expression of therapeutic genes in retinal pigment epithelial cells. Biotechnol. Bioeng. *118*, 2001–2015.

43. Fabian-Jessing, B.K., Jakobsen, T.S., Jensen, E.G., Alsing, S., Hansen, S., Aagaard, L., Askou, A.L., Bek, T., and Corydon, T.J. (2022). Animal Models of Choroidal Neovascularization: A Systematic Review. Investig. Ophthalmol. Vis. Sci. *63*, 11. https://doi.org/10.1167/iovs.63.9.11.

44. Garcá, M., Ruiz-Ederra, J., Hernández-Barbáchano, H., and Vecino, E. (2005). Topography of pig retinal ganglion cells. J. Comp. Neurol. *486*, 361–372. https://doi.org/10.1002/cne.20516.

45. Huang, J., Huang, J., Chen, Y., and Ying, G.S. (2018). Evaluation of Approaches to Analyzing Continuous Correlated Eye Data When Sample Size Is Small. Ophthalmic Epidemiol. *25*, 45–54. https://doi.org/10.1080/09286586.2017.1339809.

46. Mussolino, C., della Corte, M., Rossi, S., Viola, F., Di Vicino, U., Marrocco, E., Neglia, S., Doria, M., Testa, F., Giovannoni, R., et al. (2011). AAV-mediated photoreceptor transduction of the pig cone-enriched retina. Gene Ther. *18*, 637–645. https://doi.org/10.1038/gt.2011.3.

47. Vandenberghe, L.H., Bell, P., Maguire, A.M., Cearley, C.N., Xiao, R., Calcedo, R., Wang, L., Castle, M.J., Maguire, A.C., Grant, R., et al. (2011). Dosage thresholds for AAV2 and AAV8 photoreceptor gene therapy in monkey. Sci. Transl. Med. *3*, 88ra54. https://doi.org/10.1126/scitranslmed.3002103.

48. Khabou, H., Cordeau, C., Pacot, L., Fisson, S., and Dalkara, D. (2018). Dosage Thresholds and Influence of Transgene Cassette in Adeno-Associated Virus-Related Toxicity. Hum. Gene Ther. *29*, 1235–1241. https://doi.org/10.1089/hum.2018.144.

49. Ansari, A.M., Ahmed, A.K., Matsangos, A.E., Lay, F., Born, L.J., Marti, G., Harmon, J.W., and Sun, Z. (2016). Cellular GFP Toxicity and Immunogenicity: Potential Confounders in in Vivo Cell Tracking Experiments. Stem Cell Rev. Rep. *12*, 553–559. https://doi.org/10.1007/s12015-016-9670-8.

50. Taghizadeh, R.R., and Sherley, J.L. (2008). CFP and YFP, but not GFP, provide stable fluorescent marking of rat hepatic adult stem cells. J. Biomed. Biotechnol. *2008*, 453590. https://doi.org/10.1155/2008/453590.

51. Xiong, W., Wu, D.M., Xue, Y., Wang, S.K., Chung, M.J., Ji, X., Rana, P., Zhao, S.R., Mai, S., and Cepko, C.L. (2019). AAV cis-regulatory sequences are correlated with ocular toxicity. Proc. Natl. Acad. Sci. USA *116*, 5785–5794. https://doi.org/10.1073/pnas.1821000116.

52. Burr, A., Erickson, P., Bento, R., Shama, K., Roth, C., and Parekkadan, B. (2022). Allometric-like scaling of AAV gene therapy for systemic protein delivery. Mol. Ther. Methods Clin. Dev. *27*, 368–379. https://doi.org/10.1016/j.omtm.2022.10.011.

53. Askou, A.L., Jakobsen, T.S., and Corydon, T.J. (2021). Retinal gene therapy: an eye-opener of the 21st century. Gene Ther. *28*, 209–216. https://doi.org/10.1038/s41434-020-0168-2.

54. Clément, N., and Grieger, J.C. (2016). Manufacturing of recombinant adeno-associated viral vectors for clinical trials. Mol. Ther. Methods Clin. Dev. *3*, 16002. https://doi.org/10.1038/mtm.2016.2.

55. Jabs, D.A., Nussenblatt, R.B., and Rosenbaum, J.T.; Standardization of Uveitis Nomenclature SUN Working Group (2005). Standardization of uveitis nomenclature for reporting clinical data. Results of the First International Workshop. Am. J. Ophthalmol. *140*, 509–516. https://doi.org/10.1016/j.ajo.2005.03.057.

56. Nussenblatt, R.B., Palestine, A.G., Chan, C.C., and Roberge, F. (1985). Standardization of vitreal inflammatory activity in intermediate and posterior uveitis. Ophthalmology *92*, 467–471. https://doi.org/10.1016/s0161-6420(85)34001-0.